Contents lists available at ScienceDirect

Chemical Engineering Journal

journal homepage: www.elsevier.com/locate/cej

Metal-free bifunctional silica for conversion of waste glycerol from biodiesel: Sustainable production of formic acid

Poliane Chagas[a], Mariana A. Thibau[a], Samuel Breder[a], Patterson P. Souza[b], Gabriela S. Caldeira[b], Marcio F. Portilho[c], Cinthia S. Castro[a], Luiz C.A. Oliveira[a,*]

[a] Federal University of Minas Gerais, Department of Chemistry, Belo Horizonte 31270-901, Brazil
[b] Federal Center of Technological Education of Minas Gerais, Belo Horizonte 30421-169, Brazil
[c] CENPES – Petrobras, Cidade Universitária, Q7, Ilha do Fundão, 21949-900 Rio de Janeiro, RJ, Brazil

HIGHLIGHTS

- A sustainable route for the production of formic acid from residual glycerol.
- A synthetic SiO_2 with distinct behavior can be used directly as catalyst.
- The bifunctional catalyst character with acid and oxidizing site.
- A catalyst with high selectivity for formic acid, reaching 83% in continuous flow.

ARTICLE INFO

Keywords:
Residual glycerol
Oxidative clivage
Formic acid
Synthetic silica

ABSTRACT

This work describes for the first time the conversion of the waste glycerol from biodiesel production using a metal-free bifunctional silica with high porosity as catalyst. The mesoporous silica (synthetic SiO_2) with high specific surface area of 1489 $m^2 g^{-1}$ was used in the conversion of the residual glycerol (supplied by Petrobras, without any purification) using continuous flow (PBR) reactor. Surprisingly, this metal-free silica showed high selectivity for the oxidative cleavage product (formic acid), reaching 83% in continuous flow. This indicates that there is no need for the use of supported metals as in the most of the works in the literature, which can reduce the cost of the catalyst. The surface defects in the synthetic SiO_2 generated a high amount of Lewis acid sites (identified by pyridine adsorption experiments). Thus, the acid sites reacted *in situ* with the H_2O_2 (used as oxidizing agent during reaction for glycerol conversion), generating very active oxygen species on the catalyst surface. Therefore, the data presented in this work suggest that the prepared SiO_2 is a bifunctional catalyst that presents Lewis acid sites besides reactive oxygen species.

1. Introduction

There is currently a large volume of residual glycerol coming from the biodiesel production and, consequently, it is important to find new ways to consume this glycerol surplus [1,2]. The residual glycerol contains methanol and dissolved salts such as NaCl [3,4]. Thus, this crude glycerol should be treated to increase its purity grade, but the purification treatments (e.g., vacuum distillation and ion exchange) are often expensive [5]. In recent years, several studies investigated the transformation of the glycerol into value added products [6–9].

Glycerol can be used as raw material for various reactions such as oxidation, reduction, halogenation, dehydration and etherification and the reaction pathway depends on the catalysts properties [10,11]. Currently, there is a growing interest in the glycerol oxidation for formic acid production due to its considerable efficiency as a hydrogen carrier and direct application in fuel cells [8,12]. It is worth mentioning that the industrial production of formic acid occurs mainly through the oxidation of methane gas of fossil origin. Thus, the glycerol conversion in formic acid would be of great interest from economic and environmental point of view [13].

Xu et al. [14] studied the oxidation of glycerol to formic acid catalyzed by $Ru(OH)_4$ nanoparticles decorated on reduced graphite oxide and reached 60% yield in presence of $FeCl_3$. Farnetti et al. [8] used iron salts as homogeneous catalysts along with hydrogen peroxide for oxidation of glycerol to formic acid. Nevertheless, the authors used the high purity commercial glycerol in the catalytic tests, as in the most of

* Corresponding author.
E-mail address: lcao.ufmg@gmail.com (L.C.A. Oliveira).

https://doi.org/10.1016/j.cej.2019.03.068
Received 3 July 2018; Received in revised form 9 February 2019; Accepted 7 March 2019

the studies reported in literature [7,15,16]. It is known that impurity present in the crude glycerol substantially affects the catalysts performance, leading to different products [7,15,16].

Therefore, this work reports the conversion of the crude glycerol to formic acid catalyzed by mesoporous synthetic silica (SiO_2). The prepared silica was used directly as catalyst, without metallic active phases, which can reduce the catalyst cost. Most of the works use silica only as catalytic support for glycerol conversion (e.g. Gallium-doped silica [17] and MCM-41 silica-supported heteropolyacids [18]). Here, we observed that the H_2O_2 (used as oxidizing agent in the catalytic tests) is capable of generating oxidizing sites on the free-metal SiO_2 surface. The presence of acid and oxidant sites on the solid surface (bifunctional catalyst) was essential for the selective conversion of glycerol to formic acid, reaching high conversion and yield values.

2. Experimental part

2.1. Materials

For the synthesis of mesoporous SiO_2, the NaOH (Vetec, 95%), cetyl trimethyl ammonium bromide (CTAB, 99%, Vetec) and tetraethyl orthosilicate (TEOS, Sigma Aldrich) were used. The residual glycerol used in the reactions was provided by Petrobras-Brazil. The crude glycerol composition was determined by thermogravimetry: 6% salt, NaCl, 16% H_2O and 78% glycerol.

2.2. Synthesis of mesoporous SiO_2

The mesoporous SiO_2 was synthesized by solubilization of 16 g of CTAB in 300 mL of 0.3 mol L^{-1} NaOH solution. Then, 37 mL of TEOS was slowly dripped into the solution and the system was left under magnetic stirring for 24 h. The formed solid was filtered and washed with distilled water until pH 7. The SiO_2 was obtained by calcining at a heating rate of 10 °C min^{-1} up to 550 °C, maintaining at this temperature for 5 h.

It is interesting to note that the methodology described here was based on the methods proposed for the MCM-41 mesoporous silica [18–20]. However, the new conditions employed here do not use autoclave or long aging times which resulted in a material with distinct acidic properties and catalytic activity.

2.3. Catalysts characterization

The acidic properties of the catalyst were determined by the pyridine adsorption method. In this test, 10 mg of catalyst was placed in crucibles inside a quartz tube in a furnace and heated to 100 °C, for 2 h, under air flow (80 mL min^{-1}). After the cleaning of the surface, the pyridine was then introduced, at 50 °C. After the adsorption step, the temperature was raised to 100 °C, under air flow (80 mL min^{-1}), to remove the pyridine physisorbed on the catalyst surface. Discs of 1 cm of diameter were made under vacuum and 6 ton cm^{-2}. The infrared spectrum was acquired using a Spectrm RX, 64 scans were recorded, in a region of 1800–1400 cm^{-1}.

The quantification of acidic sites of catalyst was determined by a titration method [21]. 0.04 g synthetic SiO_2 was added into 20 mL of 0.01 mol L^{-1} NaOH solution and was stirred continuously at room temperature for 120 min. The slurry was then filtered and the supernatant was titrated using 0.01 mol L^{-1} HCl solution.

X ray diffraction (XRD) measurements were performed with a Rigaku Geigerflex diffractometer equipped with a copper tube and graphite monochromator, and diffractograms were collected at incident angles. Analysis was registred in the 2θ range of 20–70° at a scan speed of 2° min^{-1} and for the 2θ range of 1–10° at a scan speed of 0.5° min^{-1}. A N_2 adsorption/desorption isotherm was obtained at a temperature of 77 K using a Quantachrome AutosorbIQ2 equipment and pore volumes were calculated based on the adsorption branch of the isotherm using the BJH method. The specific surface area value was obtained using the BET method. To analyze the morphological structure of the synthesized materials, Transmission Electron Microscopy (TEM) images were obtained in a 2006 Tecnai G2-20-FEI microscope operating at 200 KV. The samples were dispersed in water in an ultrasonic bath for 15 min and a drop of the solution was placed on a copper support grid. After evaporation of the solvent, the grid was covered with a polymer film to protect the electron gun. Raman spectra were recorded using Sentera spectrometer at the range 40 and 3700 cm^{-1}. The instrument was equipped with laser source (532 nm) and a CCD detector.

2.4. Catalytic tests

The synthesized SiO_2 was initally tested as catalyst for degradation of hydrogen peroxide monitored by the volume of O_2 formed [$H_2O_{2(aq)} \rightarrow H_2O_{(l)} + 0.5\ O_{2(g)}$]. In this test, 50 mg of catalyst was placed in contact with 3 mL of H_2O_2 solution (50% v/v), along with 5 mL of distilled water or 5 mL of quinoline solution (500 mg L^{-1}).

The reactions for glycerol conversion were investigated in batch and continuous flow reactors. For batch operation, a stainless steel reactor was employed and the reactions were carried out using optimized conditions: 50 mg of catalyst at a fixed temperature of 150 °C and magnetic stirring at 1400 rpm. The reaction conditions were adapted from previous studies from our group [7]. The reaction products were monitored at different reaction times (30, 45, 60 and 120 min) by GC–MS (Agilent 7190 equipment). The analysis parameters were: injector temperature of 225 °C, injection volume of 1 μL, He flow of 1.3 mL min^{-1}, at a heating rate of 3 °C min^{-1}, between 90 and 150 °C and HP-5 column (5% polymethylphenylsiloxane).

The continuous flow reactions were carried out in a packed bed reactor (PBR) with dimensions of 60 × 1.5 cm (height × diameter). The reactor was filled with 46 mesh silicon carbide and 300 mg of catalyst. The feeding consisted of a mixture of 1/1 (v/v) of residual glycerol and hydrogen peroxide (30%, v/v) with a continuous flow of 0.50 mL min^{-1}. The reaction was monitored for 8 h. The reaction conditions described here are optimized conditions obtained in previous studies from our research group (as yet unpublished). The samples containing the reaction products were collected regularly at the end of the reactor and analyzed by Gas Chromatography coupled to Mass Spectrometry (GC–MS), following the same procedure described for the batch reactions.

3. Results and discussion

3.1. Characterizion of the silica catalyst

The textural properties of the synthetic silica were studied by N_2 adsorption/desorption (Fig. 1). The material presented a high specific surface area of 1489 $m^2\ g^{-1}$. The isotherm profile resemble type IV isotherm, according to IUPAC classification, which is characteristic of mesoporous materials, as confirmed by the pore size distribution (inserted figure). These data show that the material presents large pores of uniform diameter centered at 36 Å and a pore volume of 1.01 $cm^3\ g^{-1}$. The high specific surface area and, especially, the mesoporosity of the synthetic silica, indicate that this material presents great potential of use as catalyst, since large pores favor the diffusion of bulky reactant molecules. In general, this type of material is used as catalyst support due to its low catalytic activity in the absence of a metal/oxide as active phase. Herein, the synthesis conditions employed allowed obtaining a material with distinctive surface properties allowing its direct use as catalyst without metal impregnation.

Analyzing the XRD pattern at a low angle (Fig. 2), it is possible to observe a diffraction at 2θ = 2.7°, due to the (1 0 0) plane. Moreover, two weak peaks at 4.6 and 5.3° related to the (1 1 0) and (2 0 0) planes were detected. These three peaks can be attributed to a hexagonal arrangement, but with a small displacement when compared to the

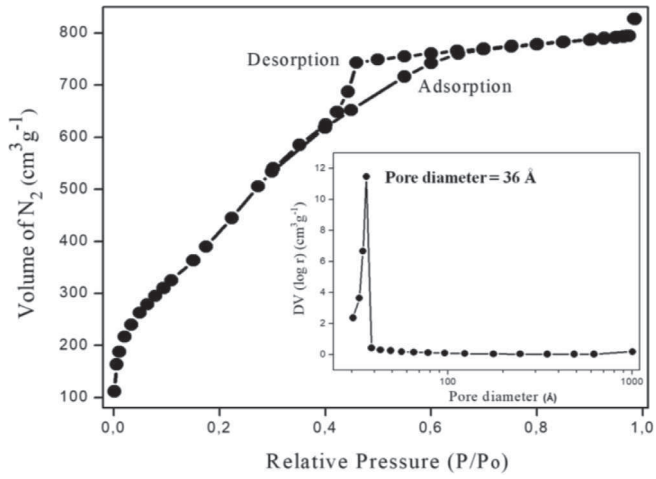

Fig. 1. N_2 adsorption/desorption isotherm at 77 K and pore size distribution for the synthetic SiO_2.

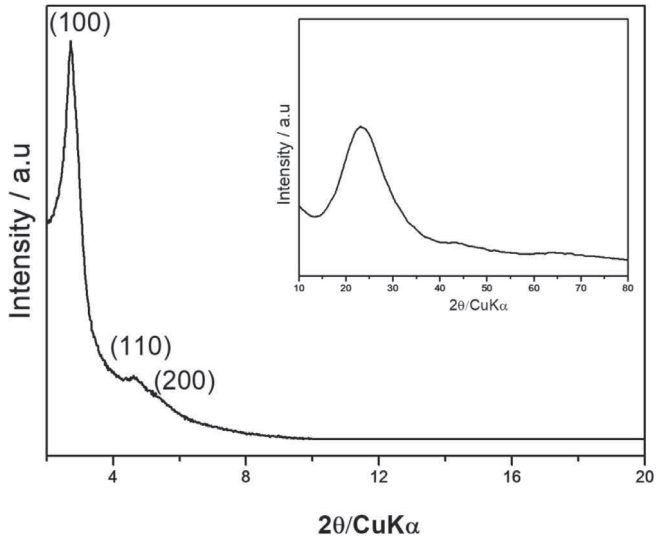

Fig. 2. Low-angle X ray diffraction pattern for the SiO_2 catalyst (2θ = 2–20°) and XRD pattern at 2θ = 10–80°.

diffractions of a typical mesoporous silica, such as MCM-41 [19,22,23]. This is indicative of a disordered hexagonal structural formation caused by the synthesis rout used here. This disordered arrangement may generate defects in the structure of the synthesized material, generating active catalytic sites, which is desirable for catalysis. The XRD patterns in the 2θ region between 10 and 80° (Fig. 2) showed only a broad peak between 15 and 38°, related to the amorphous silica structure (MCM-41-like) [19]. It is worth mentioning that although a disordered hexagonal structure of SiO_2 (MCM-41-like structure) was obtained, the methology revealed to be reproducible since the catalyst were prepared several times, maintaining the same crystalline structure and catalytic activity.

The acidity of the synthesized SiO_2 was evaluated through pyridine adsorption analyses and revealed that the material presents only Lewis acid sites. The absence of Brönsted acid sites can be due the calcination temperature (i.e., 550 °C for 5 h) and the synthesis method used. It is possible that the aging conditions, without the use of autoclave, may have contributed to obtain a silica with these particular properties. The spectrum acquired in the Infrared region showed a band at 1447 cm^{-1} (Fig. 3A), which corresponds to the coordinated pyridine at the Lewis acid sites [24–26]. These sites, which are deficient in the coordinate number, can function as surface defects where the molecules adsorb and undergo a catalytic transformation. In addition, the hydrogen peroxide (used as oxidizing agent), can be activated by that empty site leaving a highly reactive oxygen which can be a strong oxidant for organic compounds. Strong evidence that this vacant site on the SiO_2 surface reacts with H_2O_2 and is probably occupied by an activated oxygen is shown in Fig. 3A. After the H_2O_2 treatment, the synthetic silica does not present the band corresponding to the Lewis acid site (Fig. 3B). Further analyzes by Raman spectroscopy (Fig. 3C and D) corroborate these data, since the silica treated with H_2O_2 showed an evident signal at 728 cm^{-1} (number 4 peak) that is not observed for the silica without the hydrogen peroxide treatment. This signal probably refers to the Si-O bond formed by the activation with H_2O_2 at the Lewis sites, forming reactive oxygen species. The additional peaks (1, 2 and 3) are coincident with the material without peroxide treatment, indicating typical silica signals ascribed to Si-O-Si and other vibrations [27].

Quantification of the acid sites of the catalyst was determined by titration, which was 1.39 mmol g^{-1}. This total concentration was related to the concentration of Lewis acid sites, since the presence of Bronsted acid sites was not observed by the pyridine adsorption method.

To reinforce the previous proposal, H_2O_2 decomposition tests were performed in the presence of the studied catalyst. The results (Fig. 4) demonstrated that the catalyst was active for H_2O_2 decomposition. An additional H_2O_2 decomposition experiment was performed under the same conditions, however, the distilled water was replaced by a quinoline solution (500 mg L^{-1}). This is because organic compounds (such as phenol, ascorbic acid, hydroquinone, tert-butanol, etc) have affinity for the radical species such as ·OH or ·OOH. That is, if the radicals are formed in the reaction between the silica catalyst and the H_2O_2, the released volume of O_2 will be smaller. However, if the mechanism is via vacancy, the volume of O_2 formed in the absence and presence of the organic compounds will be the same [28–30].

Thus, the results suggest that the addition of the organic compound does not affect the reaction. The curve profiles (black and red lines) were very similar. This indicates that the decomposition mechanism of H_2O_2 involves vacant oxygen sites [28–31] (Fig. 4). These findings corroborate the data obtained by the pyridine adsorption method previously shown, where the Lewis acid sites correspond to vacant oxygen sites on the SiO_2 surface (Fig. 3A). Therefore, it is possible to conclude that the reaction mechanism for the synthetic SiO_2 involves the Lewis acidity, where the oxidizing groups (i.e., the reactive oxygen atoms) are created after the reaction with H_2O_2.

The catalyst was also characterized by TEM and EELS and the images are shown in Fig. 5. The analysis by electron energy-loss spectroscopy (EELS) do not show elements other than silicon. The Si edge shows a typical SiO_2 structure, Fig. 5A. The hexagonal arrangement was revealed, considering that the electronic beam was introduced along the channels (Fig. 5B). In Fig. 5C, the beam was introduced perpendicular to the axis of the channels. The structure formed by hexagonal channels observed in the TEM images corroborates the result obtained by X ray diffraction at low angles.

3.2. Catalytic tests

The reactions for glycerol conversion were investigated in batch and continuous flow reactors. The batch reaction performed under optimized conditions showed a maximum glycerol conversion of about 44%, after 60 min of reaction (Fig. 6). The GC–MS chromatogram (not shown) revealed that the major product was formic acid, with 45% selectivity, followed by 1-hydroxypropanone (34%) after 60 min of reaction (Fig. 6). It is interesting to note that the formic acid is a product of the oxidative cleavage of the glycerol [16,32,33] and the 1-hydroxypropanone is a consequence of the acidic action of the catalyst [7]. This result further attests to the bifunctional character of the prepared SiO_2. It is important to emphasize that the activation of an oxidizing agent (such as H_2O_2) by Lewis sites of pure silica is not reported

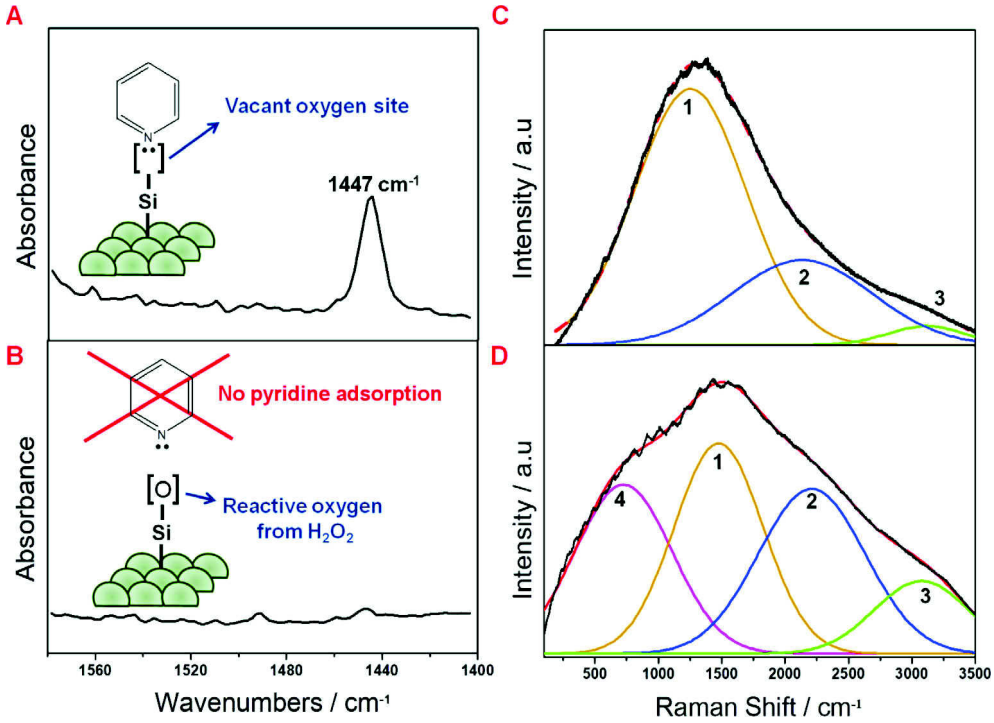

Fig. 3. Infrared spectrum after adsorption of pyridine (A) and after treatment with H_2O_2 (B) on the SiO_2 catalyst. In detail in the spectrum, a surface scheme responsible for pyridine coordinated to the Lewis acid sites (Py-L) in SiO_2. Raman spectra of silica before (C) and after the treatment with H_2O_2 (D).

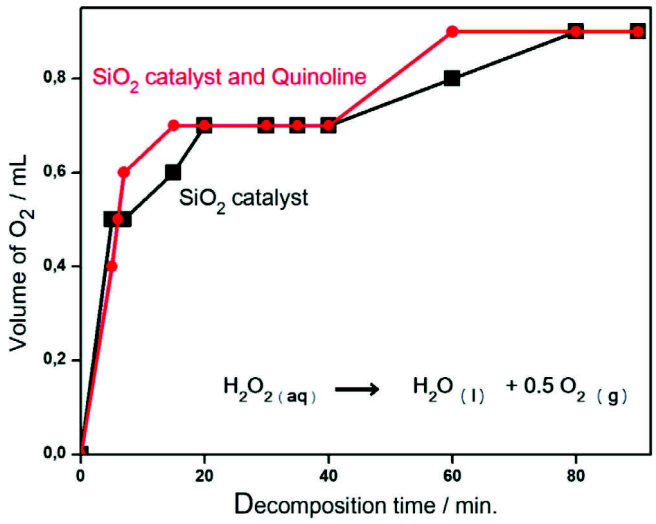

Fig. 4. O_2 formation profile from the decomposition of H_2O_2 over SiO_2 catalyst in the absence and presence of an organic compound (quinoline, 500 mg L^{-1}).

in the literature.

Considering that the large scale industrial production is generally cost effective when performed in continuous reactors rather than batch reactors, the glycerol conversion over SiO_2 catalyst was also investigated in a continuous flow system using a Packed bed reactor (PBR). The catalytic tests were carried out using the synthetic silica in the presence of hydrogen peroxide. Additionally, blank experiments were performed: (*i*) catalyst without H_2O_2 and (*ii*) only H_2O_2.

For the silica without H_2O_2 (blank *i*), a reasonable conversion (up to ≈ 50%) was observed in the first three hours of reaction (Fig. 7), possibly due to the thermal effect (150 °C) associated to the action of the acid sites present on the catalyst. However, the conversion reduced drastically afterwards (< 10% after 7 h) (Fig. 7). In the case of H_2O_2 (*ii*), the glycerol conversion was about 40% after 1 h reaction and decreased gradually to about 15% after 7 h, possibly due to the thermal decomposition of H_2O_2 during reaction (Fig. 7). Although some conversion has been obtained at the beginning of the reaction for the blank experiments, the selectivity for formic acid was quite low in both cases (≈ 9% after 7 h).

On the other hand, when the SiO_2 catalyst is used in the presence of the oxidizing agent (H_2O_2), a different result was obtained (Fig. 8A). The silica catalyst presented an almost constant conversion (≈90%) and turn over frequency (TOF) at the end of the reactor, during 8 h of reaction. This suggests that the reactor operated at steady state under the studied conditions. It is important to note that the reaction exhibited a considerable conversion over 8 h of in a continuous process, indicating that the catalyst employed here present good stability, even when using the residual glycerol containing impurities from the biodiesel production and a SiO_2 catalyst without active phases from transition metals [7,34,35].

The chromatograms (Fig. 8B) demonstrate that the reaction reached high selectivity for formic acid (≈75%) and this was maintained during the 8 h of reaction under continuous flow. Therefore, these data confirm the oxidative action of the pure silica in the presence of an oxidative agent. It was observed that the 1-hydroxypropanone, i.e., the product obtained from the acidic action of the catalyst, was formed as a minor product. On the other hand, the formic acid obtained from the oxidizing catalytic action is preserved as the major product without other reaction products being observed during 8 h of continuous flow reaction. Therefore, the results suggest that the 1-hydroxypropanone formed in contact with the Lewis acid sites is oxidized and cleaved to formic acid by the oxidizing sites formed on the catalyst surface.

The activity of the synthetic silica is quite satisfactory when compared to the literature. It important to highlight that most of the works use noble metal supported catalysts and commercial glycerol in the catalytic tests [36]. For instance, Ntho *et al.* [37] studied γ-Al_2O_3 supported Au catalysts, reaching high glycerol conversion. Xu *et al.* [14] also used a noble metal (Ru dispersed over graphene) to convert the high purity glycerol to formic acid. The gas phase dehydration of glycerol to acrolein was studied by Ma *et al.* [9], using MCM-41 supported

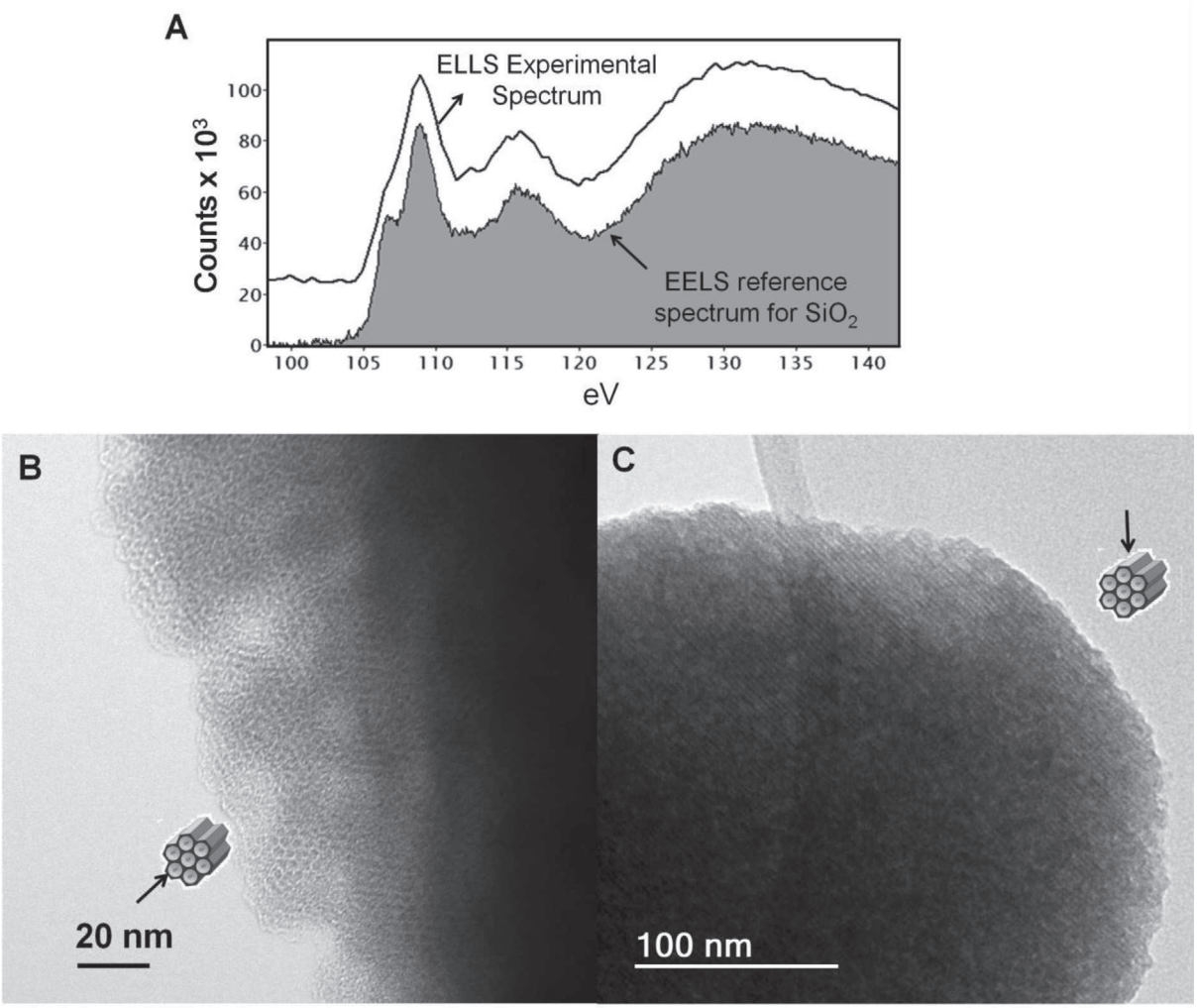

Fig. 5. A. EELS spectrum at the Si ionization edge of the SiO_2 material. Transmition Electron Microscopy (TEM) images of the SiO_2. B. The electronic beam was introduced along the channels. C. The beam was introduced perpendicular to the axis of the channels.

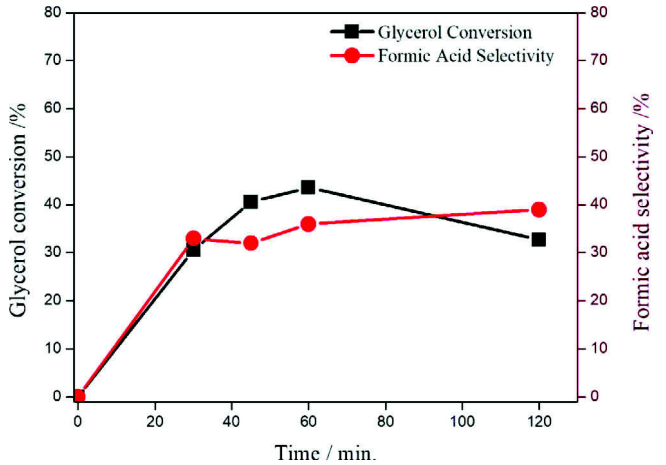

Fig. 6. Residual glycerol conversion and selectivity for formic acid in batch reactor using the SiO_2 catalyst.

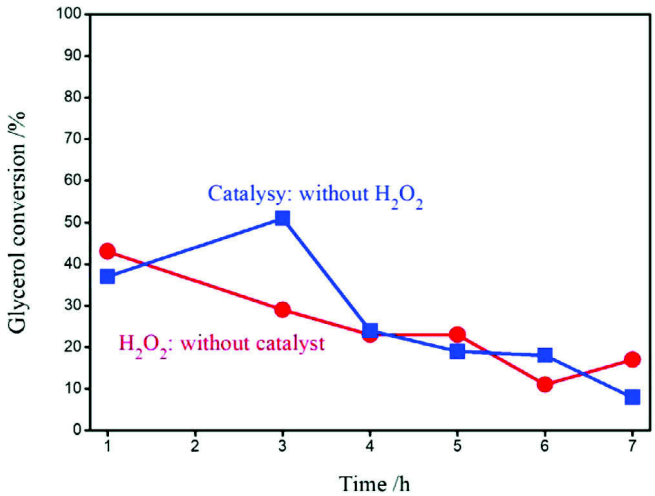

Fig. 7. Conversion of glycerol in continuous flow of the synthetic silica in the presence of hydrogen peroxide and of the blank experiments: with catalyst without H_2O_2 and only H_2O_2, without the catalyst.

phosphotungstic acids as catalysts, showing a maximum TOF of 184 h^{-1}, after 5 h of reaction. The catalytic support MCM-41 did not present acidity and showed no significant conversion [9].

One of the mechanisms proposed for the formation of formic acid from glycerol suggests that dehydration of the substrate occurs, probably on the acid sites of the catalyst. Afterwards, there are other steps involved such as the oxidation reactions (Fig. 9) [16,38–41]. In this way, a bifunctional character of the catalyst is required (acid action

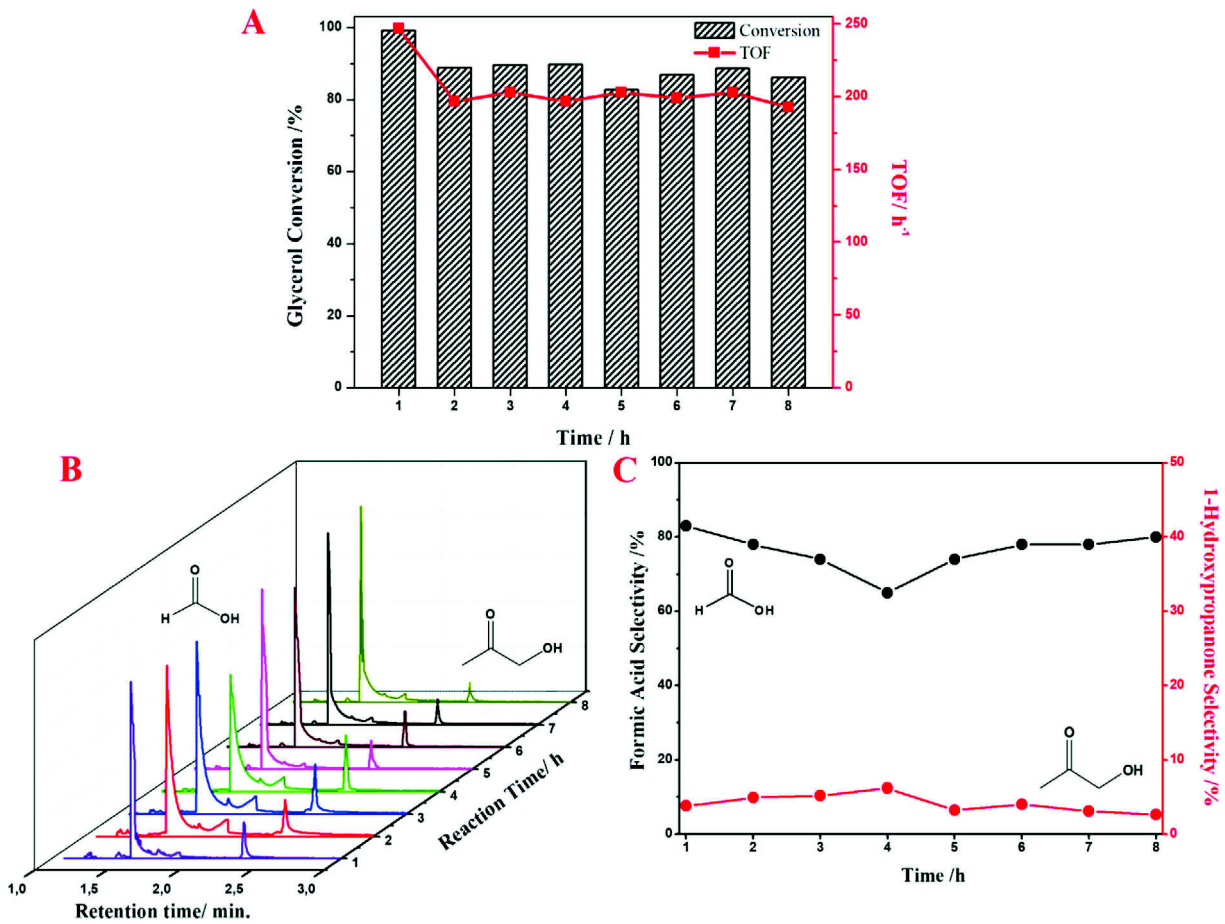

Fig. 8. A. Conversion of the glycerol and and turn over frequency (TOF) when using H_2O_2 and SiO_2. Reaction conditions: temperature of 150 °C, catalyst mass: SiO_2 = 0.30 g, reaction time: 8 h and space velocity of 59.7 h^{-1}. B. Chromatograms of conversion reactions of glycerol to formic acid in a flow reactor at 150 °C for 8 uninterrupted hours. C. Selectivity for formic acid and 1-hydroxypropanone.

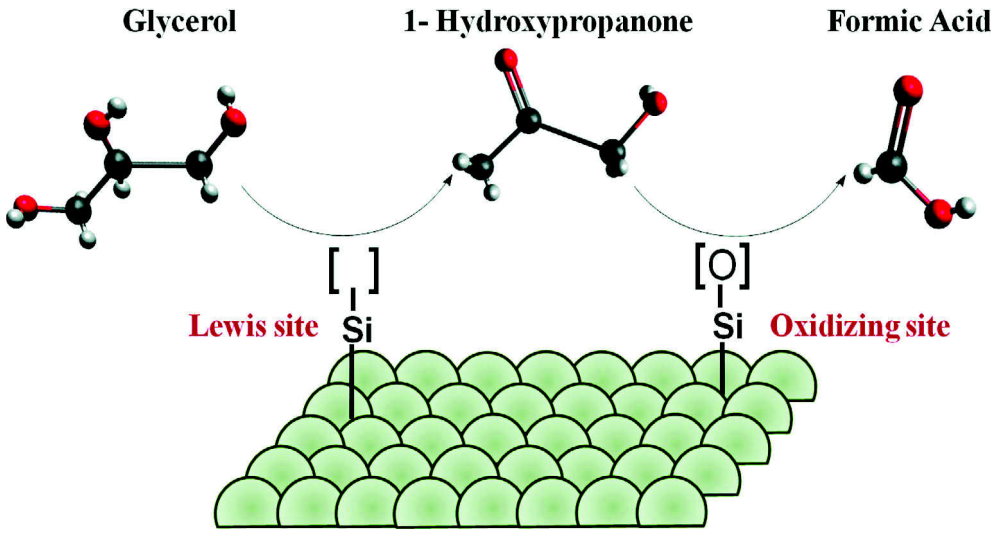

Fig. 9. Dehydration of glycerol in the Lewis acid sites of the SiO_2 catalyst and the further oxidative cleavage of 1-hydroxypropanone over the oxidizing sites generated *in situ* during the catalyst reaction with H_2O_2.

for dehydration and oxidant for cleavage) during the transformation of the glycerol to produce formic acid. After glycerol dehydration to the 1-Hydroxypropanone (compound observed in GC–MS analyzes), oxidation and cleavage occur to form formic acid (Fig. 9) [40,41].

4. Conclusion

This work presents a sustainable route for the production of formic acid (widely used commodity chemical) from residual glycerol of the biodiesel production, showing an alternative to the commercial method that employs natural gas from a non-sustainable fossil source. A pure

mesoporous SiO_2 catalyst with high surface area ($\approx 1500\,m^2\,g^{-1}$) was synthesized in a simple route and used directly as catalyst (without metal impregnation) thus considerably reducing the catalyst cost. The metal-free SiO_2 revealed to be highly active for the conversion of the waste glycerol, as generated from the biodiesel industry, without any previous purification process. The reactions in continuous flow (PBR reactor) reached conversion and TOF of approximately 60% and $200\,h^{-1}$ respectively and selectivity for formic acid of about 75%. The bifunctional character of the catalyst has been demonstrated and presents acid Lewis sites (i.e., vacant oxygen sites on the silica surface. These vacancies are able to react with H_2O_2 *in situ* during glycerol reaction thus forming highy active oxygen atoms, giving the material an oxidizing character. Thus, the synthesized material exhibits the desirable bifunctionality, acid and oxidant sites, in the conversion of glycerol to formic acid.

Acknowledgements

The authors gratefully acknowledge CAPES, CNPq and FAPEMIG for financial support, as well as the Microscopy Center-UFMG, INCT MIDAS, and Petrobras SA.

References

[1] A. Beatriz, Y.J.K. Araújo, D.L. Lima, Glycerol a Br. Hist. Appl. Synth. Stereoselective, Quim. Nova 34 (2011) 306–319.
[2] H. Duan, Y. Yamada, S. Sato, Efficient production of 1,3-butadiene in the catalytic dehydration of 2,3-butanediol, Appl. Catal. A Gen. 491 (2015) 163–169, https://doi.org/10.1016/j.apcata.2014.12.006.
[3] C.J.A. Mota, C.X.A. Da Silva, V.L.C. Gonçalves, Gliceroquímica: novos produtos e processos a partir da glicerina de produção de biodiesel, Química Nova 32 (2009) 639–648, https://doi.org/10.1590/S0100-40422009000300008.
[4] M. Anitha, S.K. Kamarudin, N.T. Kofli, The potential of glycerol as a value-added commodity, Chem. Eng. J. 295 (2016) 119–130, https://doi.org/10.1016/j.cej.2016.03.012.
[5] M.J. Haas, A.J. McAloon, W.C. Yee, T.A. Foglia, A process model to estimate biodiesel production costs, Bioresour. Technol. 97 (2006) 671–678, https://doi.org/10.1016/j.biortech.2005.03.039.
[6] M.R. Monteiro, C.L. Kugelmeier, R.S. Pinheiro, M. Otávio, S. César, Glycerol from biodiesel production: technological paths for sustainability, Renew. Sustain. Energy Rev. 88 (2018) 109–122, https://doi.org/10.1016/j.rser.2018.02.019.
[7] H.S. Oliveira, P.P. Souza, L.C.A. Oliveira, Nb and V-modified silicate for conversion of glycerol: comparison between the waste and commercial product, Catal. Today 289 (2017) 258–263, https://doi.org/10.1016/j.cattod.2016.09.012.
[8] E. Farnetti, C. Crotti, Selective oxidation of glycerol to formic acid catalyzed by iron salts, Catal. Commun. 84 (2016) 1–4, https://doi.org/10.1016/j.catcom.2016.05.014.
[9] T. Ma, J. Ding, R. Shao, W. Xu, Z. Yun, Dehydration of glycerol to acrolein over Wells-Dawson and Keggin type phosphotungstic acids supported on MCM-41 catalysts, Chem. Eng. J. 316 (2017) 797–806, https://doi.org/10.1016/j.cej.2017.02.018.
[10] J.C. Juan, J. Zhang, M.A. Yarmo, 12-Tungstophosphoric acid supported on MCM-41 for esterification of fatty acid under solvent-free condition, J. Mol. Catal. A Chem. 267 (2007) 265–271, https://doi.org/10.1016/j.molcata.2006.09.029.
[11] L.C.A. Oliveira, M.F. Portilho, A.C. Silva, H.A. Taroco, P.P. Souza, Modified niobia as a bifunctional catalyst for simultaneous dehydration and oxidation of glycerol, Appl. Catal. B Environ. 117–118 (2012) 29–35, https://doi.org/10.1016/j.apcatb.2011.12.043.
[12] L. Piola, J.A. Fernández-Salas, F. Nahra, A. Poater, L. Cavallo, S.P. Nolan, Ruthenium-catalysed decomposition of formic acid: fuel cell and catalytic applications, Mol. Catal. 440 (2017) 184–189, https://doi.org/10.1016/j.mcat.2017.06.021.
[13] C. Fellay, P.J. Dyson, G. Laurenczy, A viable hydrogen-storage system based on selective formic acid decomposition with a ruthenium catalyst, Angew. Chemie Int. Ed. 47 (2008) 3966–3968, https://doi.org/10.1002/anie.200800320.
[14] J. Xu, Y. Zhao, H. Xu, H. Zhang, B. Yu, L. Hao, Z. Liu, Selective oxidation of glycerol to formic acid catalyzed by Ru(OH)4/r-GO in the presence of FeCl3, Appl. Catal. B Environ. 155 (2014) 267–273, https://doi.org/10.1016/j.apcatb.2014.02.034.
[15] C.X.A. da Silva, C.J.A. Mota, The influence of impurities on the acid-catalyzed reaction of glycerol with acetone, Biomass Bioenergy 35 (2011) 3547–3551, https://doi.org/10.1016/j.biombioe.2011.05.004.
[16] G.S. Foo, D. Wei, D.S. Sholl, C. Sievers, Role of Lewis and brønsted acid sites in the dehydration of glycerol over niobia, ACS Catal. 4 (2014) 3180–3192, https://doi.org/10.1021/cs5006376.
[17] X. Collard, L. Li, W. Lueangchaichaweng, A. Bertrand, C. Aprile, P.P. Pescarmona, Ga-MCM-41 nanoparticles: synthesis and application of versatile heterogeneous catalysts, Catal. Today 235 (2014) 184–192, https://doi.org/10.1016/j.cattod.2014.02.055.
[18] J. Ding, M. Cui, T. Ma, R. Shao, W. Xu, P. Wang, Catalytic amination of glycerol with dimethylamine over di ff erent type of heteropolyacid /Zr-MCM-41 catalysts, Mol. Catal. 457 (2018) 51–58, https://doi.org/10.1016/j.mcat.2018.07.017.
[19] T. Ma, Z. Yun, W. Xu, L. Chen, L. Li, J. Ding, R. Shao, Pd-H3PW12O40/Zr-MCM-41: an efficient catalyst for the sustainable dehydration of glycerol to acrolein, Chem. Eng. J. 294 (2016) 343–352, https://doi.org/10.1016/j.cej.2016.02.091.
[20] T. Ma, J. Ding, R. Shao, W. Xu, Z. Yun, Dehydration of glycerol to acrolein over Wells – Dawson and Keggin type phosphotungstic acids supported on MCM-41 catalysts, Chem. Eng. J. 316 (2017) 797–806, https://doi.org/10.1016/j.cej.2017.02.018.
[21] H. Zhao, C.H. Zhou, L.M. Wu, J.Y. Lou, N. Li, H.M. Yang, D.S. Tong, W.H. Yu, Catalytic dehydration of glycerol to acrolein over sulfuric acid-activated montmorillonite catalysts, Appl. Clay Sci. 74 (2013) 154–162, https://doi.org/10.1016/j.clay.2012.09.011.
[22] C.T. Kresge, M.E. Leonowicz, W.J. Roth, J.C. Vartulli, J.S. Beck, Ordered mesoporous molecular sieves synthesized by a liquid-crystal template mechanism, Nature 359 (1992) 710–712.
[23] A. Kowalczyk, A. Borcuch, M. Michalik, B. Gil, Z. Sojka, P. Indyka, L. Chmielarz, MCM-41 modified with transition metals by template ion-exchange method as catalysts for selective catalytic oxidation of ammonia to dinitrogen, Microporous Mesoporous Mater. 240 (2017) 9–21.
[24] J. Pan, Y. Mao, H. Gao, Q. Xiong, F. Qiu, T. Zhang, Fabrication of hydrophobic polymer foams with double acid sites on surface of macropore for conversion of carbohydrate, Carbohydr. Polym. 143 (2016) 212–222, https://doi.org/10.1016/j.carbpol.2016.02.034.
[25] Y. Zhang, Q. Xiong, Y. Chen, M. Liu, P. Jin, Y. Yan, J. Pan, Synthesis of ceria and sulfated zirconia catalysts supported on mesoporous SBA-15 toward glucose conversion to 5 - hydroxymethylfurfural in a green isopropanol-mediated system, Ind. Eng. Chem. Res. 57 (2018) 1968–1979, https://doi.org/10.1021/acs.iecr.7b04671.
[26] Y. Zhang, Y. Shen, Y. Chen, Y. Yan, J. Pan, Q. Xiong, W. Shi, L. Yu, Hierarchically carbonaceous catalyst with Brønsted – Lewis acid sites prepared through Pickering HIPEs templating for biomass energy conversation, Chem. Eng. J. 294 (2016) 222–235, https://doi.org/10.1016/j.cej.2016.02.092.
[27] G. Spiekermann, M. Steele-Macinnis, C. Schmidt, S. Jahn, Vibrational mode frequencies of silica species in SiO2-H2O liquids and glasses from ab initio molecular dynamics, J. Chem. Phys. 136 (2012) 154501, , https://doi.org/10.1063/1.3703667.
[28] A.L. Teel, C.R. Warberg, D.A. Atkinson, R.J. Watts, Comparison of mineral and soluble iron Fenton's catalysts for the treatment of trichloroethylene, Water Res. 35 (2001) 977–984, https://doi.org/10.1016/S0043-1354(00)00332-8.
[29] R. Andreozzi, V. Caprio, R. Marotta, Oxidation of 3,4-dihydroxybenzoic acid by means of hydrogen peroxide in aqueous goethite slurry, Water Res. 36 (2002) 2761–2768, https://doi.org/10.1016/S0043-1354(01)00499-7.
[30] L.C.A. Oliveira, M. Gonçalves, M.C. Guerreiro, T.C. Ramalho, J.D. Fabris, M.C. Pereira, K. Sapag, A new catalyst material based on niobia/iron oxide composite on the oxidation of organic contaminants in water via heterogeneous Fenton mechanisms, Appl. Catal. A Gen. 316 (2007) 117–124, https://doi.org/10.1016/j.apcata.2006.09.027.
[31] F.G.E. Nogueira, J.H. Lopes, A.C. Silva, R.M. Lago, J.D. Fabris, L.C.A. Oliveira, Catalysts based on clay and iron oxide for oxidation of toluene, Appl. Clay Sci. 51 (2011) 385–389, https://doi.org/10.1016/j.clay.2010.12.007.
[32] W. Suprun, M. Lutecki, T. Haber, H. Papp, Acidic catalysts for the dehydration of glycerol: activity and deactivation, J. Mol. Catal. A Chem. 309 (2009) 71–78, https://doi.org/10.1016/j.molcata.2009.04.017.
[33] H. Park, Y.S. Yun, T.Y. Kim, K.R. Lee, J. Baek, J. Yi, Kinetics of the dehydration of glycerol over acid catalysts with an investigation of deactivation mechanism by coke, Appl. Catal. B Environ. 176–177 (2015) 1–10, https://doi.org/10.1016/j.apcatb.2015.03.046.
[34] Y. Ding, W. Sun, W. Yang, Q. Li, Formic acid as the in-situ hydrogen source for catalytic reduction of nitrate in water by PdAg alloy nanoparticles supported on amine-functionalized SiO2, Appl. Catal. B Environ. 203 (2017) 372–380, https://doi.org/10.1016/j.apcatb.2016.10.048.
[35] X. Collard, L. Li, W. Lueangchaichaweng, A. Bertrand, C. Aprile, P.P. Pescarmona, Ga-MCM-41 nanoparticles: synthesis and application of versatile heterogeneous catalysts, Catal. Today 235 (2014) 184–192, https://doi.org/10.1016/j.cattod.2014.02.055.
[36] D.A. Bulushev, J.R.H. Ross, Towards sustainable production of formic acid, ChemSusChem 11 (2018) 821–836, https://doi.org/10.1002/cssc.201702075.
[37] T. Ntho, J. Aluha, P. Gqogqa, M. Raphulu, G. Pattrick, Au/γ-Al2O3 catalysts for glycerol oxidation: the effect of support acidity and gold particle size, React. Kinet. Mech. Catal. 109 (2013) 133–148, https://doi.org/10.1007/s11144-013-0542-9.
[38] B. Katryniok, S. Paul, V. Belliere-Baca, P. Rey, F. Dumeignil, Glycerol dehydration to acrolein in the context of new uses of glycerol, Green Chem. 12 (2010) 2079–2098, https://doi.org/10.1039/c0gc00307g.
[39] A.K. Kinage, P.P. Upare, P. Kasinathan, Y.K. Hwang, J.S. Chang, Selective conversion of glycerol to acetol over sodium-doped metal oxide catalysts, Catal. Commun. 11 (2010) 620–623, https://doi.org/10.1016/j.catcom.2010.01.008.
[40] M.L. de Araújo, D. Mandelli, Y.N. Kozlov, W.A. Carvalho, G.B. Shul'pin, Oxidation of hydroxyacetone (acetol) with hydrogen peroxide in acetonitrile solution catalyzed by iron(III) chloride, J. Mol. Catal. A Chem. 422 (2016) 103–114, https://doi.org/10.1016/j.molcata.2016.02.011.
[41] Y. Liu, H. Tüysüz, C.-J. Jia, M. Schwickardi, R. Rinaldi, A.-H. Lu, W. Schmidt, F. Schüth, From glycerol to allyl alcohol: iron oxide catalyzed dehydration and consecutive hydrogen transfer, Chem. Commun. 46 (2010) 1238, https://doi.org/10.1039/b921648k.

物 理 化 学 学 报
Acta Phys. -Chim. Sin. **2018,** *34* (8), 886–895

[Article] doi: 10.3866/PKU.WHXB201711151 www.whxb.pku.edu.cn

Selective Oxidation of Glycerol with Hydrogen Peroxide Using Silica-Encapsulated Heteropolyacid Catalyst

YUAN Mingming, LI Difan, ZHAO Xiuge, MA Wenbao, KONG Kang, NI Wenxiu, GU Qingwen, HOU Zhenshan *

Key Laboratory for Advanced Materials, Research Institute of Industrial Catalysis, School of Chemistry & Molecular Engineering, East China University of Science and Technology, Shanghai 200237, P. R. China.

Abstract: The Keggin type heteropolyacids (HPAs) have attracted increasing attention due to their strong Bronsted acidity and excellent redox properties, which could play an important role in accelerating the conversion of bio-derived molecules. In this work, heteropolyacid (HPA, $H_4PMo_{11}VO_{40}$) encapsulated by silica was synthesized by a sol-gel method and a sequential silylation technique (HPA@SiO_2-N_2-S). The as-synthesized material was characterized by Fourier transform infrared spectroscopy (FT-IR), X-ray diffraction (XRD), thermogravimetric analysis (TGA), scanning electron microscope (SEM) and transmission electron microscopy (TEM). The FT-IR spectra show that the HPA anions preserved their Keggin structure when incorporated into the catalyst. The XRD patterns show that HPA molecules are uniformly dispersed within the silica network. The SEM and TEM images confirm that the catalyst was composed of spherical nanometer-sized particles. The porous properties of the catalysts measured by the N_2 adsorption-desorption isotherms indicate that the Brunauer, Emmett and Teller (BET) surface area of pure SiO_2 was 287 $m^2 \cdot g^{-1}$, but upon encapsulation of HPA into the silica matrix, a lower surface area (245 $m^2 \cdot g^{-1}$) was measured for the resulting material. In addition, the pore diameter was reduced after silylation. Furthermore, the hydrophobicity of the catalysts was investigated by the measurement of contact angle (CA) with water. The SiO_2 and SiO_2/HPA catalysts were completely hydrophilic and the contact angle was close to 0°. However, the contact angle of the silylated catalyst was determined to be 137°, indicating that the silylation procedure significantly increased the hydrophobicity of the catalyst. The as-prepared catalysts were also used as heterogeneous catalysts for the selective oxidation of glycerol. The prepared material exhibited excellent catalytic activity towards glycerol oxidation, in which the glycerol can be selectively transformed into formic acid (*ca.* 70% selectivity) and glycolic acid (*ca.* 27% selectivity) using H_2O_2 as an oxidant under mild reaction conditions. The effect of the silylation procedure on the recyclability of catalyst was also investigated in this work. The characterizations described above indicated that silylation procedure can significantly increase the hydrophobicity and limit the pore sizes, resulting in high leach-resistance towards HPA, thus improving the recyclability of the silica-encapsulated HPA catalyst, as compared to the SiO_2/HPA catalyst prepared with the conventional impregnation method. Furthermore, the conversion in the second catalytic run is even higher than that of the initial run, which is likely because more active sites are exposed after the first run. The catalyst can be reused for at least five cycles without any leaching of HPA. The spent catalyst did not undergo structural changes, as revealed by FT-IR, XRD, and SEM characterization. Moreover, it was found that the strong Bronsted acid additives played a crucial role in the catalytic oxidation of glycerol.

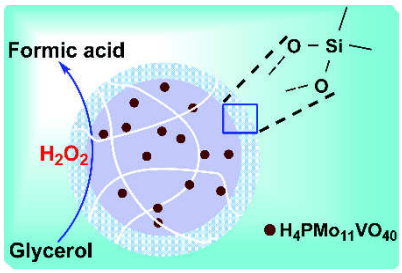

Key Words: Glycerol oxidation; Heteropolyacid; Encapsulation; Formic acid; Hydrogen peroxide

Received: October 27, 2017; Revised: November 10, 2017; Accepted: November 10, 2017; Published online: November 15, 2017.

*Corresponding author. Email: houzhenshan@ecust.edu.cn; Tel.: +86-21-64251686.

The project was supported by the National Natural Science Foundation of China (21373082, 21773061) and the Innovation Program of Shanghai Municipal Education Commission, China (15ZZ031).

国家自然科学基金项目(21373082, 21773061)和上海市教委科研创新项目(15ZZ031)资助

二氧化硅包覆的杂多酸在双氧水存在条件下催化氧化甘油

袁明明，李迪帆，赵秀阁，马文保，孔康，倪文秀，顾青雯，侯震山*

教育部结构可控先进功能材料及其制备重点实验室，工业催化研究所，华东理工大学化学与分子工程学院，上海 200237

摘要：催化剂的酸性和氧化还原性在催化生物质平台分子转化过程中起着非常重要的作用，杂多酸具有较强的酸性以及优良的氧化还原性，因而杂多酸在生物质催化转化领域备受关注。本文利用溶胶-凝胶法和硅烷化方法将杂多酸催化剂封装在二氧化硅载体内部，随后以傅立叶红外光谱、X-射线衍射仪、热重分析仪、透射电子显微镜、扫描电镜等手段对合成的材料进行了表征。红外光谱表明杂多酸在催化剂中保持了其完整结构，X-射线衍射表明杂多酸高度分散在二氧化硅载体上，电镜表征显示催化剂呈球形纳米颗粒形貌。基于以上表征结果，我们将包覆的杂多酸催化剂应用于甘油氧化，在以过氧化氢为氧化剂，温和反应条件下，合成的材料对甘油氧化具有良好的催化活性，其中对甲酸的选择性大约为70%，对乙醇酸的选择性大约为27%。硅烷化过程对于催化剂循环起着重要的作用，单纯二氧化硅的比表面积为287 $m^2 \cdot g^{-1}$，二氧化硅包覆杂多酸经过硅烷化后，其比表面积降为245 $m^2 \cdot g^{-1}$，而且孔径也有所降低。单纯二氧化硅与水的接触角为0°，而二氧化硅包覆的杂多酸在硅烷化之后的催化剂具有很强的疏水性，与水的接触角为137°。根据这些催化剂表征数据说明硅烷化过程不仅可以显著提高催化剂的疏水性，而且同时限制了载体孔径，阻止杂多酸流失到反应体系中，与传统的浸渍法将杂多酸负载在二氧化硅载体上得到的催化剂相比，催化剂的循环利用性显著提高。反应后的催化剂结构与新鲜催化剂相比，并没有发生明显变化。催化剂经过一次循环后，表面暴露了更多的活性中心，活性稍有提高。催化剂在反应体系中加入强质子酸可以显著提高反应的催化性能，揭示了Bronsted酸在甘油氧化过程中对甘油分子的活化起着重要的作用。

关键词：甘油氧化；杂多酸；封装；甲酸；过氧化氢

中图分类号：O643

1 Introduction

Due to the depletion of fossil fuels and the improvement of awareness of environmental protection, biodiesel resources have been receiving extensive worldwide attention and are being rapidly flourished because of their excellent renewability, environmental performance, and innocuous advantages [1–3]. Biodiesel is the best known in biofuels, obtained through the transesterification between vegetable oils and short chain alcohols with a catalytic process [4]. The glycerol in an amount of *ca.* 10% (*w*, mass fraction) of the overall biodiesel production is generated as a by-product in this process, which has been identified as an important platform compounds for producing high value chemicals [5]. Representative reaction pathways for the glycerol valorization contain hydrodeoxygenation, hydrogenation, hydrogenolysis, oxidation and dehydration etc. Among these various utilization approaches, the glycerol oxidation is highly attractive, which can provide C1 products such as formic acid (FA), C2 products such as glycolic acids (GCA) and oxalic acid (OA), and many C3 products such as tartronic acid, glyceraldehyde, glyceric acid, and dihydroxyacetone. These products are all high-added chemical intermediates and are still being obtained through expensive processes or any other way [6–8]. Among the routes for the utilization of these chemicals, the increasing interest in efficient FA production aims at its application as hydrogen carrier [9,10]. As FA owns 4.4% hydrogen content and some well-known systems could decompose it under mild conditions to hydrogen and carbon dioxide [11–13]. Additionally, FA is also a convenient source of C1 raw material for the chemical synthesis. For example, the efficient hydrogenation/ disproportionation of formic acid (FA) to methanol by using iridium catalysts has been reported recently [14].

Over the past decades, the selective oxidation of glycerol has been conducted to obtain valuable products with molecular oxygen. The seminal studies have founded that supported gold catalyst have high selectivity and conversion for glycerol oxidation [15–17]. In addition, the aerobic oxidation of glycerol has been widely studied using noble metal such as Pt [18,19], Pd [20] *etc.* In these catalytic systems, the noble metals play a key role in glycerol oxidation and the catalytic performance depends on the basicity of the reaction medium. However, due to its basicity, it produces a lot of organic acid salts and thus the mixture after reaction needs further neutralization and acidification so as to obtain the target products. In addition to its basicity, the other disadvantage is that the supported noble metal catalysts are rather expensive for the further practical application and also tend to lose activity rapidly due to the oxidation of metal surface and thus result in the poisoning of the active sites [21]. Therefore, the design of other catalyst systems was becoming a hot point in the current research field.

On the other hand, hydrogen peroxide has been widely used as an oxidant in organic oxidation reactions owing to its

environmentally friendly nature in that the degradation products of hydrogen peroxide are only oxygen and water [22]. Hydrogen peroxide is strong oxidant which can oxidize a broad variety of inorganic and organic substrates in liquid-phase reactions under very mild reaction conditions [23]. Hence, the catalytic oxidation of glycerol has been carried out by using the hydrogen peroxide as an oxidant recently [24–26].

The catalyst acidity could play a very important role in accelerating the hydrolysis of glycerol molecules [27,28]. The Keggin type heteropolyacids (HPAs) have attracted increasing attention due to their strong Bronsted acidity and environmental friendliness [29–31]. Meanwhile, HPAs also showed excellent redox properties [32]. Their low surface area (< 10 $m^2 \cdot g^{-1}$) and high solubility in polar solvents limit its potential catalytic application. For example, HPAs have been employed as efficient catalysts in aqueous media for the oxidation of glycerol into FA, but the separation of homogenous HPA catalysts was tedious due to miscibility of HPAs and FA with water media [33].

Generally, the heterogeneous catalysts have some particular advantages over homogeneous ones, for example, the solid catalysts can be removed easily from the reaction media and thus recycled. From this point of view, solid catalysts usually represent a better option in liquid phase reaction. On the basis of discuss above, in this work, we attempted to immobilize HPA ($H_4PMo_{11}VO_{40}$) within silica matrix via a sol-gel method and the sequential silylation technique, which offered an appropriate hydrophobicity and also shielding of HPA, suppressing the leaching of HPA and but allowing penetration of reactants and products through porous silica during the aqueous reaction. It was found that the as-obtained catalyst exhibited excellent activity and reusability for glycerol oxidation using H_2O_2 as an oxidant under very mild conditions.

2 Experimental

2.1 Materials

Disodium hydrogen phosphate, sodium metavanadate, sulfuric acid, sodium molybdenum oxide, ethyl ether, dimethyl sulfoxide, tetraethyl orthosilicate, acetonitrile, glycerol, toluene, dimethyldichlorosilane were purchased from Sinopharm Chemical Reagent Co., Ltd., Shanghai. Distilled water used in this work was produced by our own laboratory. High purity N_2 (99.999%) was supplied by ShangNong Gas Factory. All other chemicals (analytical grade) were from Sino pharm Chemical. Toluene (analytical grade) was dried by using the standard methods.

2.2 Catalyst preparation

2.2.1 Preparation of $H_4PMo_{11}VO_{40}$ (HPA)

In a typical synthesis route, 0.71 g of disodium hydrogen phosphate was dissolved in 10 mL of water, and then 0.61 g of sodium metavanadate that had been dissolved by boiling in 10 mL of water was mixed with the above solution under stirring. The cooled mixture was acidified with 0.5 mL of concentrated sulfuric acid to a red color. 11.26 g of sodium molybdenum was dissolved in 20 mL of water, and added to this mixture. Finally, 8.5 mL of concentrated sulfuric acid was slowly dropped into the previously prepared aqueous solution with vigorous stirring. In the process, the dark red color changed to a lighter red and the pH of the solution was 1–2. The water solution was cooled and the heteropolyacid extracted with 40 mL of ethyl ether [34]. In the extraction process, it will be divided into three layers and the heteropoly etherate was present in the middle layer. After separation, a stream of air was passed through the heteropoly etherate layer to free it of ether, which offered the orange solid powder as HPA (3.70 g).

2.2.2 Preparation of SiO_2-encapsulated HPA catalyst

Absolute ethanol (10 mL) was mixed with distilled water (0.12 g), then add tetraethyl orthosilicate (1.6 mL) into the mixture. Allowed the solution standing for thirty minutes and followed by adding dimethyl sulfoxide solution (4 mL) containing HPA (0.1 g); in the end, added 4 mL of $NH_3 \cdot H_2O$ (28%). After 2 h, the as-obtained gel was dried. The sample was designated as HPA@SiO_2 sample. Additionally, silica gel (SiO_2) was prepared by the same method besides HPA was not added.

2.2.3 The silylation of HPA@SiO_2

Surface silylation of silica was carried out using dimethyldichlorosilane as the silylation agents. The procedures for surface modification of silica with the agents were similar to that in the literature [35]. 0.8 mmol of dimethyldichlorosilane was dissolved in 10.0 mL of dried toluene. 0.2 g of dried HPA@SiO_2 composite was dispersed in the above solution. After stirring for 20 min at 80 °C under a N_2 atmosphere, the solid was isolated through filtrated, thoroughly washed with toluene for several times. The obtained product was dried for 12 h at 100 °C under vacuum. Then, the dried sample followed by calcination at 250 °C for 1 h in a nitrogen reduction furnace prior to reaction. This sample was named as HPA@SiO_2-S-N_2. The elemental analysis gave that the actual loading of HPA was about 13%. The as-synthesized silica gel (SiO_2) support was impregnated conveniently with HPA to afford 13% HPA/SiO_2 catalyst.

2.3 Catalyst characterization

XRD analysis of types samples were performed in the 2θ range of 10°–80° on an D/MAX 2550 VB/PC instrument (Rigaku Corporation, Japan) using a graphite crystal a monochromator. The textural properties from N_2 adsorption isotherms were obtained on NOVA 2200e equipment (Quantachrome, USA). The surface area was obtained from the isotherms in the relative pressure range of 0.0–0.35. Pore volume was determined at p/p_0 of 0.99. The inductively coupled plasmaatomic emission spectroscopy ICP-AES (Inductively Coupled Plasma-Atomic Emission Spectroscopy) analysis was carried out on a ICP-710ES instrument (Varian Company, Germany). The sample was putted in a nickel crucible mixed with some sodium hydroxide and then putted into muffle at 500 °C for 30 min to destroy the structure of sample, followed by dissolving with water. FT-IR spectra were recorded from pressed KBr pellets at room temperature on a Magna550

(Nicolet, USA). A spectrum of dry KBr was also recorded as background. The thermal stability of catalysts was determined by TGA method (heating rate: 10 °C·min^{-1}; N_2 flow, 100 mL·min^{-1}) using Perkin Elmer Pyris Diamond Analyser (Netzsch, Germany). The SEM images were performed on JSM electron microscopes (JEOL JSM-6360LV, Japan). TEM was performed in a JEM 2010 instrument (JEOL Corporation, Japan) operating at 200 kV with a nominal resolution of 0.25 nm. The samples for TEM were prepared by dropping the aqueous solutions containing the NPs onto the carbon-coated Cu grids. Water contact angle (CA) was carried out by the Contact Angle Meter (CA100C, Innuo Company, Shanghai, China) using the droplet profile as a method. The CA was determined using a tangent placed at the intersection of the liquid and solid. A water droplet with a volume of 2 μL was dispensed by a piezo doser onto each sample disk.

The amount of acid sites of the different samples was obtained with temperature programmed desorption of ammonia (NH_3-TPD). About 0.15 g of catalyst was loaded in a quartz tube. Prior to each test, the sample was pre-treated in He at 300 °C for 1 h, cooled to 50 °C to remove surface water. Then, the sample was maintain at 50 °C for 1 h and saturated with a 10% NH_3-in-N_2 mixture, and then flushed by He for 1 h to remove physically adsorbed ammonia. Then, the sample was heated to 400 °C at a heating rate of 10 °C·min^{-1} in the same flow of He. The profiles of desorption were recorded using a thermal conductivity detector (TCD, Vodo, Zhejiang, China).

2.4 Catalytic reaction

The oxidation of glycerol was carried out as follows. A mixture of glycerol (1.25 mmol), acetonitrile (0.90 mL), 30% aqueous H_2O_2 (6.25 mmol), and the HPA@SiO_2-S-N_2 catalysts (0.06 g) were placed in a 25 mL Schlenk flask equipped with a magnetic stirrer and then stirred at 70 °C for 12 h. When the reaction was finished, the mixtures were filtrated by centrifugation. The resulting supernatant liquid was diluted 5 times with distilled water and analyzed by HPLC using LC-100 chromatograph equipped with a Aminex HPX-87H Column (300 × 7.8 mm, Bio-Rad Company, USA) used with a solution of 0.005 mol·L^{-1} H_2SO_4 (0.5 mL·min^{-1}) as the eluent at 55 °C. The recovered catalyst washed with ethanol and toluene for several times and dried in a vacuum at 60 °C for recycling tests. The conversion of glycerol and selectivity towards products were calculated as follows:

$$\text{Conversion}\,(\%) = \frac{\text{amount of glycerol converted (mole)}}{\text{total amount of glycerol (mole)}} \times 100\%$$

$$\text{Selectivity}\,(\%) = \frac{\text{amount of product (mole)}}{\text{amount of glycerol converted (mole)}} \times \frac{\text{number of carbon atoms in the product}}{3} \times 100\%$$

$$\text{Carbon mass balance}\,(\%) = \frac{\text{carbon atoms found in the liquid products (mole)}}{\text{total carbon atoms in the feed (mole)}} \times 100\%$$

Hot filtration experiment for the HPA@SiO_2-S-N_2 catalyst was performed with two parallel experiments. The procedures were given by the following procedures: a mixture of glycerol (1.25 mmol), acetonitrile (0.88 mL), 30% aqueous H_2O_2 (6.25 mmol), and 0.06 g catalyst was placed in a 25 mL Schlenk flask equipped with a magnetic stirrer and condenser, followed by stirring at 70 °C. Two parallel experiments were performed without or with separating the catalyst from the hot reaction mixture after 8 h [36]. Hot filtration experiment for the HPA/SiO_2 catalyst was carried out in a similar method except that the catalyst was isolated after 50 min.

3 Results and discussion

3.1 Catalyst characterization

In this work, the HPA was introduced conveniently into the silica by a sol-gel procedure, followed by the silylation approach. The preparation route has been depicted briefly in Scheme 1.

The obtained samples were first characterized by FT-IR. A small band observed at 1635 cm^{-1} and a broad band at 3420 cm^{-1} was due to absorbed water in Fig. 1a–e. The pure HPA showed IR spectra with the specific bands of the Keggin structure as shown in Fig. 1a, which showed band at 1062 cm^{-1} (ν_{as} P—Oa), 961 cm^{-1} (ν_{as} Mo=O_d), 867 cm^{-1} (ν_{as} Mo—O_b—Mo), and 777 cm^{-1} (ν_{as} Mo—Oc—Mo), 591 cm^{-1} (δ P—O), respectively. These absorptions are constant with the Keggin structure of the heteropolyanion [37]. As shown in Fig. 1b, SiO_2 showed the vibration band at 1095 cm^{-1}, 950 cm^{-1}, 800 cm^{-1} and 584 cm^{-1}, which can be assigned to ν_{as} (Si—O—Si), ν (Si—O), ν_s (Si—O—Si) and δ (Si—O—Si) bonds, recpectively [38]. After the HPA was introduced into the silica matrix, the specific bands of the Keggin structure showed a slight change, as compared with that of the parent HPA. It was noted that bands of HPA/SiO_2 and

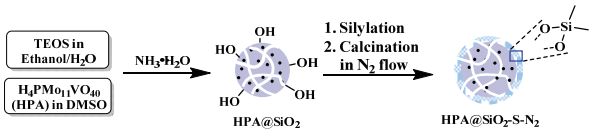

Scheme 1 The preparation approach of the silica-encapsulated HPA catalyst.

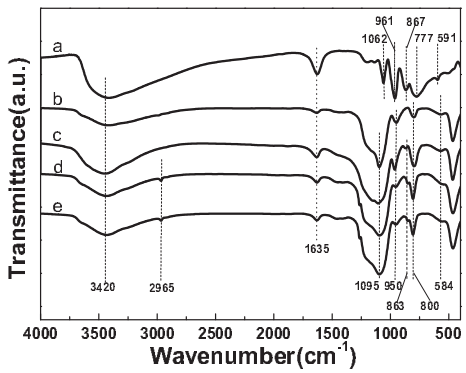

Fig. 1 FT-IR spectra of (a) HPA; (b) SiO_2; (c) HPA/SiO_2 catalyst; (d) the fresh HPA@SiO_2-S-N_2 catalyst; (e) the HPA@SiO_2-S-N_2 catalyst after reused for 5 times.

HPA@SiO_2-S-N_2 catalyst in the 1200–400 cm^{-1} region were completely or partially overlapped by that of SiO_2. For example, the band assigned to the P—O asymmetric stretching vibration at 1062 cm^{-1} of HPA is completely overlapped by the strong band at 1095 cm^{-1} of SiO_2 (Fig. 1c–e), while the two strong bands appeared in the spectra of HPA/SiO_2 and HPA@ SiO_2-S-N_2 appeared at 950 and 800 cm^{-1}, as a result of the overlapping of the absorption bands of silica and HPA. However, the asymmetric stretching vibration band at 863 cm^{-1} that assigned to Mo—O_b—Mo vibration, which was not found in SiO_2, but it indeed appeared in SiO_2-encapsulated/supported HPA catalysts (Fig. 1c–e). Additionally, a well defined band appeared at 2965 cm^{-1} after silylation in Fig. 1d–e can be assigned to C—H stretching vibration in surface —CH_3 groups [39]. All these results indicated clearly that HPA has been embedded within silica matrix and also the silylation was successful by dimethyldichlorosilane.

The XRD patterns of the obtained catalysts were depicted in Fig. 2. The most intensive reflections of bulk HPAs appear in the following range: 7°–10°, 17°–23° and 26°–32° (Fig. 2a), which are characteristic of the Keggin structure [40], while HPA/SiO_2 and HPA@SiO_2-S-N_2 catalysts did not give obvious diffraction peak and only displayed a large and flat diffraction peak appeared at 2θ = 15°–35°, which was assigned to amorphous silica (Fig. 2a–2e), which evidenced that bulk HPA did not form but HPA was highly dispersed on in the SiO_2 support.

The porous properties of the catalysts were measured by the

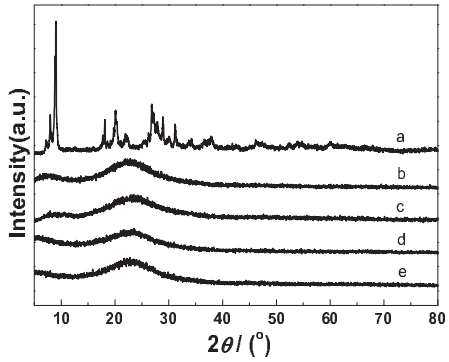

Fig. 2 X-ray diffraction patterns of (a) HPA; (b) SiO_2; (c) HPA/SiO_2 catalyst; (d) the fresh HPA@SiO_2-S-N_2 catalyst; (e) the HPA@SiO_2-S-N_2 catalyst after reused for 5 times.

N_2 adsorption-desorption isotherms method (Fig. S1). As shown in Table 1, the BET surface area of pure SiO_2 was 287 $m^2 \cdot g^{-1}$ (Table 1, entry 1), the encapsulation of HPA into the silica matrix resulted in a lower surface area (Table 1, entries 3–5). But their surface areas are still higher than that of the catalyst prepared by impregnation (Table 1, entry 2). Interestingly, the encapsulation of HPA into silica matrix could result in the increase of pore diameter (Table S1, entries 1 *vs.* 2 and 3), possibly arising from the effect of bulky HPA molecules. In the next, the hydrophobicity of the catalysts has been investigated by the measurement of contact angle (CA). The SiO_2 and HPA/SiO_2 was completely hydrophilic and the contact angle was close to 0° (Table 1, entries 1 and 2). However, SiO_2-encapsulated HPA catalyst (HPA@SiO_2) showed slightly stronger hydrophibicity, as compared with that of SiO_2 and HPA/SiO_2 samples likely due to the difference in surface morphology. Especially, the silylated catalyst even gave a larger CA (Table 1, entry 4). As a result, the silylation procedure can increase obviously the hydrophobicity of the catalysts. Furthermore, the pore diameter reduced rationally after silylation, as compared with that of the patent catalyst (Table S1, entries 2 *vs.* 3).

Subsequently, the surface morphology of catalysts was examined by SEM. As shown in Fig. 3, the SEM images showed that the structure of SiO_2 is spherical (Fig. 3a and d), and HPA/SiO_2 catalyst maintained the morphology of the SiO_2 but we can see some particles on the surface (Figs. 3b and e). When the HPA was encapsulated into the silica by a sol-gel procedure, the SEM images showed that the structure of HPA@SiO_2 catalyst is spherical but showed rougher surface (Fig. 3c and f). After silylation, the images of HPA@SiO_2-S-N_2 (Fig. 3g and i) catalyst were similar to that of HPA@SiO_2 catalyst. Interestingly, the HPA encapsulation into SiO_2 through the sol-gel method can reduce the size of SiO_2 particles significantly and the silylation did not influence the surface morphology. As discussed above, the encapsulation of HPA into SiO_2 (HPA@SiO_2) can result in stronger hydrophobicity, as compared with that of HPA/SiO_2, which could be attributed to the smaller particle size and the different surface morphology [41,42].

In the next, the TEM images showed that the structure of

Table 1 Physicochemical properties and catalytic performances of the oxidation of glycerol using different catalysts [a]

Entry	Catalyst	Surface area/($m^2 \cdot g^{-1}$)	CA/(°)	Conversion/% [b]	Selectivity/% [b]		
					FA	GCA	others
1	SiO_2	287	0	0	–	–	–
2	HPA/SiO_2	175	0	76(5)	66(45)	27(14)	7(41)
3	HPA@SiO_2	261	96	61(28)	68(54)	27(22)	5(24)
4	HPA@SiO_2-S-N_2	245	134	34(51)	70(74)	27(22)	3(4)
5[c]	HPA@SiO_2-S-N_2	245	134	40	67	–	33

[a] Reaction conditions: 1.25 mmol of glycerol, 6.25 mmol of 30% aqueous H_2O_2, 0.88 mL CH_3CN, 0.06 g catalyst, T = 70 °C, t = 12 h. FA = formic acid; GCA = glycolic acid; [b] The values in the parentheses represented the conversion or selectivity in the second run. [c] GCA as a substrate. The carbon mass balance for the glycerol oxidation was normally more than 85%.

HPA/SiO_2 is spherical with about 150 nm diameter (Fig. 4a), while the structure of HPA@SiO_2-S-N_2 catalyst is spherical with about 12 nm diameter Fig. 5g, which was in well agreement with that of SEM images (Fig. 3b *vs.* 3g). Energy-dispersive X-ray spectrometry (EDS) elemental mapping analysis (Figs. 4 and 5) validated the immobilization of Mo species had a tendency to be distributed around silica particles on HPA/SiO_2 catalyst (Fig. 4e and f) but highly uniform dispersity within HPA@SiO_2-S-N_2 catalyst (Fig. 5e and f).

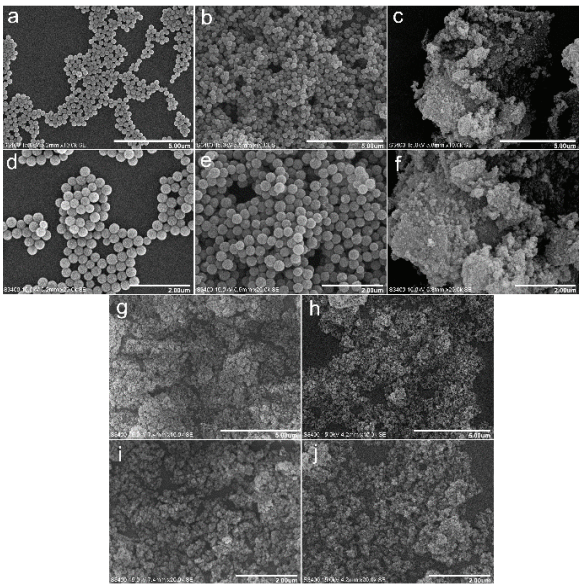

Fig. 3 SEM images of (a, d) SiO_2; (b, e) HPA/SiO_2; (c, f) HPA@SiO_2; (g, i) the fresh HPA@SiO_2-S-N_2 catalyst; (h, j) HPA@SiO_2-S-N_2 catalyst after reused for 5 times.

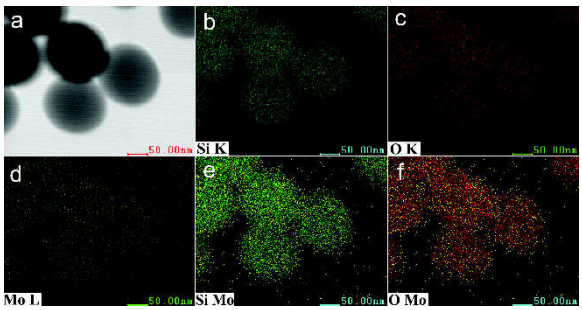

Fig. 4 TEM images of HPA/SiO_2 (a), and elemental mapping images of Si (b), O (c), Mo (d), Si and Mo (e), O and Mo (f).

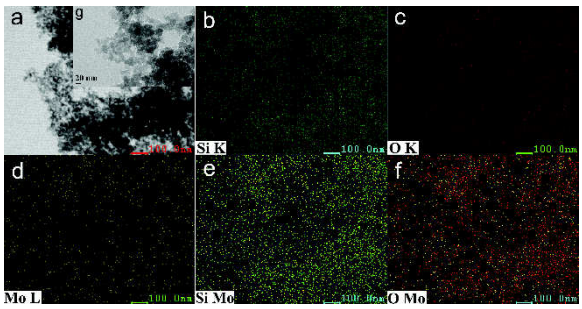

Fig. 5 TEM image of HPA@SiO_2-S-N_2 (a, g), and elemental mapping images of Si (b), O (c), Mo (d), Si and Mo (e), O and Mo (f).

The temperature-programmed desorption of ammonia (NH_3-TPD) is a useful method to provide general information about the strength distribution of acid sites of solid acids. According to the desorption temperature of the absorbed ammonia, the strength of solid acid sites are formally assigned as weak and strong. The NH_3-TPD curves of the samples were shown in Fig. 6. The NH_3-TPD patterns of both HPA@SiO_2-S-N_2 and HPA@SiO_2 catalysts showed only a desorption peaks in similar temperature regions (50–200 °C). On the other hand, HPA/SiO_2 samples exhibited an over-lapping peak including two peaks around 200 °C and 340 °C, respectively [43]. This indicated that HPA/SiO_2 showed a stronger surface acidity than that of HPA@SiO_2-S-N_2 and HPA@SiO_2, which was understandable because HPA was mainly loaded on surface silica for HPA/SiO_2, leading to more accessible adsorption of NH_3 molecules, as compared with that of silica-encapsulated HPA catalysts.

The thermal stability of the catalysts was investigated by TGA. As shown in Fig. S2, both SiO_2 and HPA@SiO_2-S-N_2 showed a slight weight loss below 120 °C, which could be attributed to the removal of the adsorbed H_2O on the surface of SiO_2 and the HPA@SiO_2-S-N_2. Increasing temperature from 120 °C to 700 °C, it was seen that SiO_2 only afforded a slight weight loss from 98% to 95%, which could be assigned to the increase of siloxane bridges (Si—O—Si) because of the condensation of isolated silanol groups [44]. The HPA@SiO_2-S-N_2 catalyst gave a weight loss from 95% to 85.5% in the range of 300° to 700°, which was mainly attributed to the removal of gradual degradation of methyl on the surface of SiO_2.

3.2 Catalytic performance

The as-prepared catalysts have been tested for the glycerol oxidation reaction. As shown in Table 1, except SiO_2 other catalysts were all active for the oxidation of glycerol reaction (Table 1, entries 2–4). However, they exhibited different catalytic activity although the loading amounts of the HPA were same. The fresh HPA/SiO_2 catalyst showed high catalytic performance for glycerol oxidation, but HPA on catalyst surface is not stable and was visually leached into reaction media after reaction, resulting in yellow effluent and thus giving very poor activity in the second run (Table 1, entry 2). The HPA@SiO_2

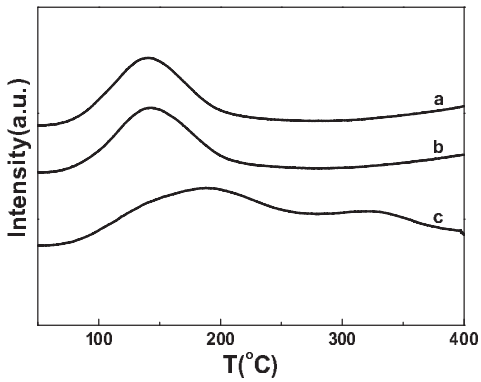

Fig. 6 NH_3-TPD profiles of the (a) HPA@SiO_2-S-N_2 catalyst; (b) HPA@SiO_2; (c) HPA/SiO_2 catalyst.

catalyst showed some improvement for catalyst recyclability, but the obvious decrease of activity was still observed in the second run (Table 1, entry 3). However, after the HPA@SiO_2 sample was silylated and then calcined at 250 °C under the N_2 flow, the as-obtained catalyst HPA@SiO_2-S-N_2 can be recyclable and even the catalytic activity became better in the second run (Table 1, entry 4), which might be attributed obviously to the strong hydrophobicity and reducing pore sizes, resulting in shielding of HPA, suppressing the leaching of HPA and but allowing penetration of reactants and products through porous silica during the oxidation reaction. Obviously, the higher catalytic activity of fresh HPA/SiO_2 could be related with these easy accessible strong acidic sites, as presented at NH_3-TPD spectra (Fig. 6).

The effects of reaction condition (temperature, reaction time, amounts of catalyst) were investigated over the HPA@SiO_2-S-N_2 catalyst. Firstly, the effect of the reaction temperature was shown in Fig. 7a, which indicated that the reaction temperature had a crucial impact on the reaction. It was found that the conversion of glycerol increased continuously and reached a maximum but that decreased above 70 °C, resulting from the decomposition of H_2O_2 under higher temperature. Additionally, the selectivity to FA kept unchanged but the selectivity to GCA decreases above 70 °C, indicating that GCA could be converted into FA under higher temperature. The parallel experiment with GCA as a substrate show ed that GCA indeed can be oxidized into FA in 40% of conversion and 67% selectivity under the same conditions (Table 1, entry 5).

The effect of reaction time was obtained from Fig. 7b. Under the condition of 70 °C, the conversion of glycerol had a gradual increase within the first 5 h and then had a rapidly increment between 5 h and 10 h. However, longer reaction time could result in the decrease of FA and GCA selectivity. This can be explained that FA and GCA can be degraded further into CO_2, which has been confirmed by GC-MS (7890A-5975C, Agilent, USA), showing that the gas samples indeed contained CO_2, but no CO was detected from formic acid decomposition. Hence, the optimal reaction time is 12 h. Last, the influence of amounts of catalyst on the oxidation reaction of glycerol was also examined at 70 °C for 12 h. As shown in Fig. 7c, the conversion of glycerol was increased with the increase of catalyst until 0.06 g, in which can eliminate the influence of diffusion. The following reaction has been performed according to the conditions above.

Because acidity site has a crucial effect on catalytic activity, the impact of different acid additives on catalytic activity has been evaluated for the glycerol oxidation with H_2O_2. The results were listed in Table 2, which illustrated that Lewis acids used in this work almost did not influence the conversion of glycerol at all (Table 2, entries 2–4), but Bronsted acid additives can improve the conversion of glycerol significantly (Table 2, entries 5–9). Among of them, CF_3SO_3H is the most active acid from either conversion, or selectivity to FA (Table 2, entry 9). The control experiments indicated that when only acid additives were employed for glycerol oxidation, most of acids only offered low activity for glycerol conversion (Table S2, entries 1–7). CF_3SO_3H gave moderate activity (Table S2, entry 8), but the combination of CF_3SO_3H and HPA@SiO_2-S-N_2 catalyst exhibited much higher catalytic performance (Table 2, entry 9). These results proved unambiguously that strong Bronsted acid played a critical role in enhancing the activity and selectivity of glycerol oxidation over HPA@SiO_2-S-N_2 catalyst.

On the base of the results above, HPA@SiO_2-S-N_2 catalyst showed the highest catalytic performance. Hence, HPA@SiO_2-S-N_2 catalyst, was employed for the oxidation of the other biomass platform molecules including ethylene glycol, glucose, sorbitol, fructose, xylitol and 1, 2-propanediol. As shown in

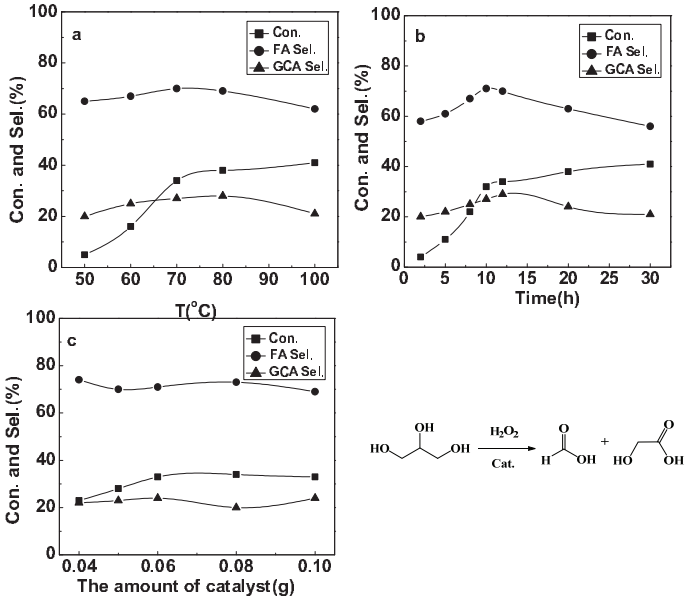

Fig. 7 Dependence of glycerol conversion and selectivity on the reaction condition over HPA@SiO_2-S-N_2 catalyst.

Table 3, ethylene glycol, glucose and sorbitol had a low reactivity (Table 3, entries 1–3), while fructose, 1, 2-propanediol and xylitol had a relatively high conversion (Table 3, entries 4–6) in the absence of any acid additive. When CF_3SO_3H was added as an additive, all biomass-derived molecules afforded higher conversion, although the selectivity to FA was variable (Table 3, entries 1–6). For example, the conversion of fructose improved from 60% to 100% and selectivity to FA from 48% to 62% due to the addition of CF_3SO_3H. It was noting that although only CF_3SO_3H afforded the moderate conversion (Table S3) for the oxidation of the other biomass platform molecules in the absence of th e HPA@SiO_2-S-N_2 catalyst, but the activity was much lower that of the combined CF_3SO_3H and HPA@SiO_2-S-N_2 catalysts (Table 3, entries 1–6). These results indicated that Bronsted acid additives can enhance conversion of other biomass-derived molecules through acid hydrolysis for this reaction [28].

Table 2 Different acid additives for the oxidation of glycerol reaction over HPA@SiO_2-S-N_2 catalyst [a].

Entry	Additives	Conversion/%	Selectivity/%		
			FA	GCA	others
1	none	34	70	27	3
2	$AlCl_3$	33	63	28	9
3	$ZnCl_2$	34	66	19	15
4	$InCl_3$	37	69	23	8
5	HCl	46	72	17	11
6	*p*-$CH_3(C_6H_4)SO_3H$	42	81	18	1
7	H_2SO_4	45	56	14	30
8	$(CF_3SO_2)_2NH$	55	63	13	24
9	CF_3SO_3H	52	81	17	2

[a] Reaction conditions: 1.25 mmol of glycerol, 6.25 mmol of 30% aqueous H_2O_2, 0.88 mL CH_3CN, 0.06 g catalyst, acid = 0.5 mmol. T = 70 °C, t = 12 h. FA = formic acid; GCA = glycolic acid. The carbon mass balance for the glycerol oxidation was normally more than 90%.

3.3 Catalyst stability

The reusability of the HPA@SiO_2-S-N_2 catalysts was examined under the optimized conditions (Fig. 8). After reaction, the solid catalyst was recovered conveniently by simple centrifugation, followed by washing with ethanol and toluene for several times. And then it was dried at 60 °C under the vacuum. Then the recovered catalyst was reused for the next recycle. At first, the reusability of HPA@SiO_2-S-N_2 catalyst was evaluated. It was found that the catalyst could be reused for at least five times with high conversion and selectivity to FA. It is worth noting that the conversion in the second run is even higher than that of the initial activity but remained unchanged as starting from the second recycle while the selectivity of the product remained the same (Fig. 8a). In contrast, after strong Bronsted acid CF_3SO_3H was added to the reaction system, the conversion of glycerol and selectivity to formic acid kept high and did not change obviously during the consecutive five recycle (Fig. 8b). These results strongly suggested that strong Bronsted acid, as well as redox sites is important for glycerol activation, and HPA@SiO_2-S-N_2 catalyst could expose more active sites after the first run, and thereby increasing contact area of the catalyst and substrates, which can be proved by a loss of hydrophobicity

Table 3 Different substrates for the oxidation reaction catalyzed by HPA@SiO_2-S-N_2 catalyst [a].

Entry	Substrates	Conversion/%	Selectiviy/%						
			FA	GCA	IS	LA	AA	GA	others
1	Ethylene glycol	31 (59)	15 (81)	47 (0)	–	0 (0)	0 (5)	0 (0)	37 (14)
2	Glucose	25 (78)	67 (51)	0 (12)	–	0 (0)	0 (3)	0 (0)	33 (34)
3	Sorbitol	29 (72)	57 (53)	0 (9)	26 (2)	0 (0)	0 (0)	0 (14)	17 (22)
4	Fructose	60 (100)	48 (62)	17 (31)	–	7 (0)	0 (2)	0 (0)	28 (5)
5	1,2-Propanediol	54 (76)	45 (44)	23 (2)	–	0 (0)	0 (45)	0 (0)	32 (9)
6	Xylitol	48 (81)	54 (67)	0 (10)	–	0 (0)	25 (5)	8 (12)	13 (6)

[a] Reaction conditions: 1.25 mmol of glycerol, 6.25 mmol of 30% aqueous H_2O_2, 0.88 mL CH_3CN, 0.06 g catalyst, T = 70 °C, t = 12 h. FA=formic acid; GCA = glycolic acid; IS = isosorbide; LA= lactic acid; AA = acetic acid; GA= glyoxylic acid. The values in the parenthesis denoted the conversion or selectivity with CF_3SO_3H (0.5 mmol) as an additive.

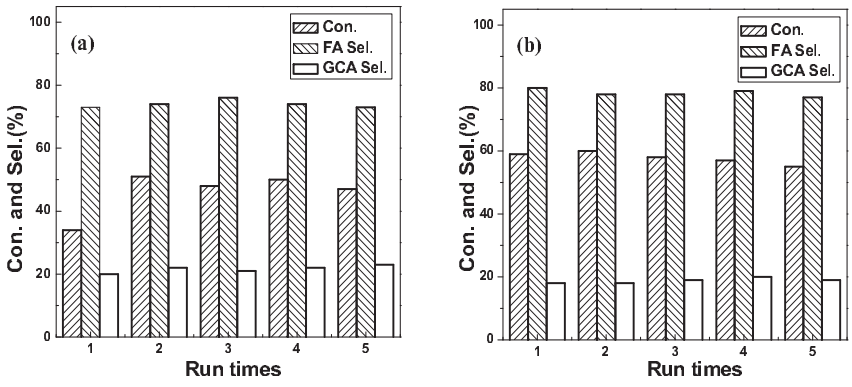

Fig. 8 Recyclability of (a) HPA@SiO_2-S-N_2 catalyst without CF_3SO_3H as an additive; (b) HPA@SiO_2-S-N_2 catalyst with CF_3SO_3H (0.5 mmol) as an additive.

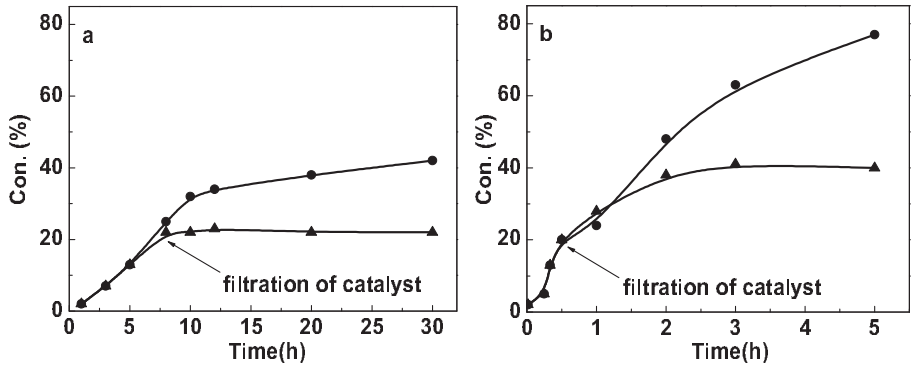

Fig. 9 Hot filtration experiments for the glycerol oxidation with H_2O_2 over (a) HPA@SiO_2-S-N_2 catalyst; (b) HPA/SiO_2 catalyst.

Solid square points (●): without isolating catalyst; Solid triangle points (▲): with isolating catalyst and then reaction in the filtrate.

arising from a partial removal of methyl group of silica surface by oxidation reaction (Fig. S3c *vs.* d).

The spent catalyst has also been examined for the possible structural changes. The characteristic vibration bands of heteropolyanions with the Keggin structure at 1095, 950, 863, 800 and 584 cm^{-1} were observed in FT-IR spectrum of the used HPA@SiO_2-S-N_2 (Fig. 1d and e), indicating that the structure of the heteropolyanion remains intact. The XRD pattern of the reused catalyst was also in agreement with that of fresh one (Fig. 2d and e). The surface morphology of the reused catalyst was shown in Fig. 3h and j, which indicated that the catalyst was still spherical and the morphology of the catalyst did not undergo obvious changes after reaction. The spent HPA@SiO_2-S-N_2 catalyst still showed hydrophobicity (CA = 114°), although the water CA decreased slightly, as compared with that of the fresh one.

According to the above discussion, there came the idea that whether the present catalytic reaction went through a heterogeneous way or not. Thus, the fast hot filtration at the reaction temperature was employed to examine the filtrate for activity. For HPA@SiO_2-S-N_2 catalyst, as shown in Fig. 9a, no further glycerol was converted once the catalyst was removed, which evidenced unambiguously that the catalytically active species was not present in the homogeneous filtrate. Finally, the possible leaching of HPA into media after the catalytic reaction was determined by ICP-AES, which showed that no P, Mo and V species were found in effluents under our reaction conditions. This result proved that the catalytic reaction proceeded over HPA@SiO_2-S-N_2 catalyst by a heterogeneous mechanism. However, for HPA/SiO_2 catalyst, as shown in Fig. 9b, because of the leaching of heteropolyacid active species into filtrate, there was still further glycerol was converted in the filtrate after the catalyst was removed.

4 Conclusions

In this work, we employed a sol-gel method and sequential silylation technique to encapsulate HPA into silica to afford an insoluble and easily separable heterogeneous catalyst. The as-prepared HPA@SiO_2-S-N_2 catalyst could be reused for at least five times with high conversion and showed no HPA leaching. The silylation procedure obviously increased the hydrophobicity but reduced the pore sizes, which led to high leach-resistance of HPAs during the consecutive reaction runs. Under the best reaction conditions, the conversion of the glycerol can be reached 50% and the selectivity to formic acid was 70% and to glycolic acid 27% by using H_2O_2 as an oxidant, respectively. In addition, the addition of strong Bronsted acid into the reaction system can improve the catalytic activity significantly, which indicated that Bronsted acid sites have an important impact on activating glycerol molecule during the glycerol oxidation reaction.

Supporting Information: available free of charge *via* the internet at http://www.whxb.pku.edu.cn.

References

(1) Deuss, P. J.; Scott, M.; Tran, F.; Westwood, N. J.; Vries, J. G.; Barta, K. *J. Am. Chem. Soc.* **2015,** *137* (23), 7456. doi: 10.1021/jacs.5b03693

(2) Chheda, J. N.; Huber, G. W.; Dumesic, J. A. *Angew. Chem. Int. Ed.* **2007,** *46* (38), 7164. doi: 10.1002/anie.200604274

(3) Xu, S.; Zhou, P.; Zhang, Z.; Yang, C.; Zhang, B.; Deng, K.; Bottle, S.; Zhu, H. *J. Am. Chem. Soc.* **2017,** *139* (41), 14775. doi: 10.1021/jacs.7b08861

(4) Lange, J, P. *Angew. Chem. Int. Ed.* **2015,** *54* (45), 13186. doi: 10.1002/anie.201503595

(5) Zhu, S. H.; Wang, J. G.; Fan, W. B. *Acta Phys. -Chim. Sin.* **2016,** *32* (1), 85. [朱善辉, 王建国, 樊卫斌. 物理化学学报, **2016,** *32* (1), 85.] doi: 10.3866/PKU.WHXB201511061

(6) Bozell, J. J.; Petersen, G. R. *Green Chem.* **2010,** *12* (4), 539. doi: 10.1039/b922014c

(7) Brandner, A.; Lehnert, K.; Bienholz, A.; Lucas, M.; Claus, P. *Top. Catal.* **2009,** *52* (3), 278. doi: 10.1007/s11244-008-9164-2

(8) Gallezot, P. *Chem. Soc. Rev.* **2012,** *41* (4), 1538. doi: 10.1039/c1cs15147a

(9) Loges, B.; Boddien, A.; Junge, H.; Beller, M. *Angew. Chem. Int. Ed.* **2008,** *47* (21), 3962. doi: 10.1002/anie.200705972

(10) Gilkey, M. J.; Xu, B. J. *ACS Catal.* **2016,** *6* (3), 1420. doi: 10.1021/acscatal.5b02171

(11) Boddien, A.; Mellmann, D.; Gaertner, F.; Jackstell, R.; Junge, H.; Dyson, P. J.; Laurenczy, G.; Ludwig, R.; Beller, M. *Science* **2011,** *333* (6050), 1733. doi: 10.1126/science.1206613

(12) Yu, W. Y.; Mullen, G. M.; Flaherty, D. W.; Mullins, C. B. *J. Am. Chem. Soc.* **2014,** *136* (31), 11070. doi: 10.1021/ja505192v

(13) Barnard, J. H.; Wang, C.; Berry, N. G.; Xiao, J. *Chem. Sci.* **2013,** *4* (3), 1234. doi: 10.1039/c2sc21923a

(14) Tsurusaki, A.; Murata, K.; Onishi, N.; Sordakis, K.; Laurenczy, G.; Himeda, Y. *ACS Catal.* **2017,** *7* (2), 1123. doi: 10.1021/acscatal.6b03194

(15) Villa, A.; Dimitratos, N.; Chan-Thaw, C. E.; Hammond, C.; Prati, L.; Hutchings, G. J. *Acc. Chem. Res.* **2015,** *48* (5), 1403. doi: 10.1021/ar500426g

(16) Dodekatos, G.; Tüysüz, H. *ChemCatChem.* **2017,** *9* (4), 610. doi: 10.1002/cctc.201601219

(17) D'Agostino, C.; Brett, G.; Divitini, G.; Ducati, C.; Hutchings, G. J.; Mantle, M. D.; F. Gladden, L. F. *ACS Catal.* **2017,** *7* (7), 4235. doi: 10.1021/acscatal.7b01255

(18) Tsuji, A.; Rao, K. T.; Nishimura, S.; Takagaki, A.; Ebitani, K. *ChemSusChem* **2011,** *4* (4), 542. doi: 10.1002/cssc.201000359

(19) Rodrigues, E. G.; Pereira, M. F. R.; Chen, X.; Delgado, J. J.; Órfão, J. J. M. *Ind. Eng. Chem. Res.* **2013,** *52* (49), 17390. doi: 10.1021/ie402331u

(20) Sankar, M.; Dimitratos, N.; Knight, D. W.; Carley, A. F.; Tiruvalam, R.; Kiely, C. J.; Thomas, D.; Hutchings, G. J. *ChemSusChem.* **2009,** *2* (12), 1145. doi: 10.1002/cssc.200900133

(21) Davis, S. E.; Ide, M. S.; Davis, R. J. *Green Chem.* **2013,** *15* (1), 17. doi: 10.1039/c2gc36441g

(22) Campos-Martin, J. M.; Blanco-Brieva, G.; Fierro, J. L. *Angew. Chem. Int. Ed.* **2006,** *45* (42), 6962. doi: 10.1002/anie.200503779

(23) Wang, S. S; Popovic, Z.; Wu, H. H; Liu, Y. *ChemCatChem.* **2011,** *3* (7), 1208. doi: 10.1002/cctc.201000401

(24) Sarkar, B.; Pendem, C.; Konathala, L. N. S.; Tiwari, R.; Sasaki, T.; Bal, R. *Chem. Commun.* **2014,** *50* (68), 9707. doi: 10.1039/c4cc03842h

(25) Faroppa, M. L.; Musci, J. J.; Chiosso, M. E.; Caggiano, C. G.; Bideberripe, H. P.; Fierro, J. L. G.; Siri, G. J.; Casella, M. L. *Chin. J. Catal.* **2016,** *37* (11), 1982. doi: 10.1016/S1872-2067(16)62531-7

(26) Corrado Crotti, C.; Farnetti, E. *J. Mol. Catal. A-Chem.* **2015,** *396*, 353. doi: 10.1016/j.molcata.2014.10.021

(27) Niu, M.; Hou, Y.; Ren, S.; Wu, W.; Marsh, K. N. *Green Chem.* **2015,** *17* (1), 453. doi:10.1039/C4GC01440E

(28) Huang, Y. B.; Fu, Y. *Green Chem.* **2013,** *15* (5), 1095. doi: 10.1039/C3GC40136G

(29) Lan, J. H.; Lin, J. C.; Chen, Z. C.; Yin, G. C. *ACS Catal.* **2015,** *5* (4), 2035. doi: 10.1021/cs501776n

(30) Lachkar, D.; Vilona, D.; Dumont, E.; Lelli, M.; Lacote, E. *Angew. Chem. Int. Ed.* **2016,** *55* (20), 5961. doi: 10.1002/anie.201510954

(31) Ma, Q.; Tong, J. H.; Su, L. D.; Wang, W. H.; Ma, W. M.; Bo, L. L. *Acta Phys. -Chim. Sin.* **2016,** *32* (12)，2961. [马青, 童金辉, 宿玲弟, 王文慧, 马文梅, 薄丽丽. 物理化学学报, **2016,** *32* (12), 2961.] doi: 10.3866/PKU.WHXB201609181

(32) Okuhara, T. *Chem. Rev.* **2002,** *102* (10), 3641. doi: 10.1021/cr0103569

(33) Lu, T.; Niu, M.; Hou, Y.; Wu, W.; Ren, S.; Yang, F. *Green Chem.* **2016,** *18* (17), 4725. doi: 10.1039/c6gc01271j

(34) George, B.; Tsigdinos, A.; Hallada, C. J. *Inorg. Chem.* **1968,** *7* (3), 437. doi: 10.1021/ic50061a009

(35) Zhao, X. S.; Lu, G. Q.; Whittaker, A. K.; Millar, G. J.; Zhu, H. Y. *J. Phys. Chem. B.* **1997,** *101*, 6525. doi: 10.1021/jp971366

(36) Sheldon, R. A.; Wallau, M.; Arends, I. W. C. E.; Schuchardt, U. *Acc. Chem. Res.* **1998,** *31* (8), 485. doi: 10.1021/ar9700163

(37) Jing, L.; Shi, J.; Zhang, F.; Zhong, Y. J.; Zhu, W. D. *Ind. Eng. Chem. Res.* **2013,** *52* (30), 10095. doi: 10.1021/ie4007112

(38) Dippong, T.; Leveib, E. A.; Cadarb, O.; Mesarosc, A.; Borodid, G. *J. Anal. Appl. Pyrol.* **2017,** *125*, 169. doi: 10.1016/j.jaap.2017.04.005

(39) Capel-Sanchez, M. C.; Barrio, L.; Campos-Martin, J. M.; Fierro, J. L. G. *J. Colloid Interface Sci.* **2004,** *277* (1), 146. doi: 10.1016/j.jcis.2004.04.055

(40) Jing, F.; Katryniok, B.; Dumeignil, F.; Bordes-Richard, E.; Paul, S. *Catal. Sci. Technol.* **2014,** *4* (9), 2938. doi: 10.1039/c4cy00518j

(41) Feng, L.; Zhang, Y, N.; Xi, J. M.; Zhu, Y.; Wang, N.; Xia, F.; Jiang, L. *Langmuir* **2008,** *24* (8), 4114. doi: 10.1021/la703821h

(42) Feng, X. Q.; Gao, X. F.; Wu, Z. N.; Jiang, L.; Zheng, Q. S. *Langmuir* **2007,** *23* (9), 4892. doi: 10.1021/la063039b

(43) Viswanadham, B.; Jhansi, P.; Chary, K. V. R.; Friedrich, H. B.; Singh, S. *Catal. Lett.* **2016,** *146* (2), 364. doi: 10.1007/s10562-015-1646-9

(44) Zhao, K. Y.; Wang, X. H.; Chen, T.; Wu, H.; Li, J. G.; Yang, B. X.; Li, D. Y.; Wei, J. F. *Ind. Eng. Chem. Res.* **2017,** *56* (9), 2549. doi: 10.1021/acs.iecr.6b03015

materials

MDPI

Review

Porous Silicon-Based Catalysts for the Dehydration of Glycerol to High Value-Added Products

Juan Antonio Cecilia, Cristina García-Sancho *, Carmen Pilar Jiménez-Gómez, Ramón Moreno-Tost and Pedro Maireles-Torres

Universidad de Málaga, Departamento de Química Inorgánica, Cristalografía y Mineralogía (Unidad Asociada al ICP-CSIC), Facultad de Ciencias, Campus de Teatinos s/n, 29071 Málaga, Spain; jacecilia@uma.es (J.A.C.); carmenpjg@uma.es (C.P.J.-G.); rmtost@uma.es (R.M.-T.); maireles@uma.es (P.M.-T.)

* Correspondence: cristinags@uma.es; Tel.: +34-952132373; Fax: +34-952131870

Received: 29 June 2018; Accepted: 27 August 2018; Published: 31 August 2018

Abstract: Increasing worldwide biodiesel production has led to the generation of an important glycerol surplus, which needs to be valorized in order to improve the economic and environmental sustainability of the biodiesel industry. In this context, glycerol dehydration to acrolein by acid catalysis appears to be a potential route of glycerol valorization, since acrolein is an important intermediate for many chemical industries. The main drawback of this catalytic process is catalyst deactivation. Different alternatives have been proposed for overcoming it, such as the use of mesoporous materials in order to facilitate the diffusion of glycerol and reaction products, thus minimizing deactivation. This review compiles the main achievements of the use of mesoporous silica-containing materials that have been deployed either as a catalyst or for support in glycerol dehydration to acrolein. Thus, the effect of mesoporosity on both catalytic performance and deactivation will be discussed, as well as the blocking of pores by coke deposition.

Keywords: mesoporous silica; glycerol; dehydration; acid catalysis; acrolein

1. Introduction

The growth of the world population, as well as improvement in quality of life, have caused an exponential consumption of fossil resources in the last century. This has led to their depletion, so it the search and development of alternative energy sources to replace them efficiently is necessary. Among them, biomass is the only sustainable source from which energy, fuels, and chemicals can be obtained [1]. Currently, the governments are legislating stringent regulations in which traditional fuels must be blended with biofuels in order to decrease emissions associated with fossil fuels. In this regard, the European Union aims to have 10% of the transport fuel coming from renewable sources in order to reduce greenhouse gas emissions [2]. Among them, the most important biofuels, in terms of production and mature industrial technologies, are bioethanol and biodiesel. In this latter case, it is produced from the transesterification process of vegetable oils or animal fats with short-chain alcohols, mainly methanol, under either base or acid catalysis, using homogeneous or heterogeneous conditions (Figure 1).

Biodiesel is an environmentally friendly fuel with a relatively low greenhouse effect, because of the lower pollutant gases and particulate matter emissions. In addition, biofuels avoid sulfur emissions and the formation of polycyclic aromatic hydrocarbons, and they are biodegradable in comparison to traditional fossil fuels [3,4].

The triglycerides used for the synthesis of biodiesel (Table 1) are traditionally obtained from several oleaginous plants, such as soybean, palm, sunflower or rapeseed. However, these vegetable oils are also used in food industries; therefore, they must not be considered as sustainable raw materials,

since they could increase speculation, social imbalances, and the over-exploitation of fertile zones. Thus, the search for alternative oils is necessary, which should not interfere with the food chain. In this sense, an alternative feedstock for the synthesis of biodiesel is used as cooking oil, which is a waste without commercial interest.

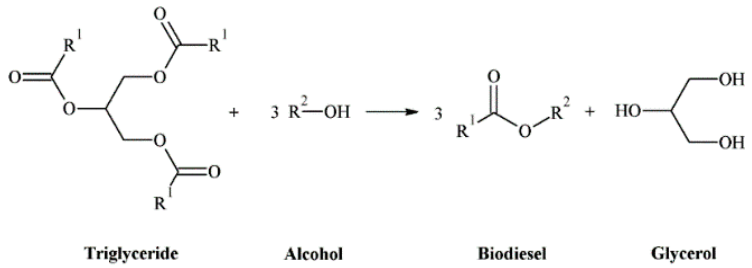

Figure 1. Transesterification reaction for biodiesel synthesis.

Table 1. Current feedstocks for biodiesel production, based on Tan et al. [5].

Feedstock	Types	Remarks
First generation	- Palm oil - Rapeseed - Soybean oil - Sunflower oil - Peanut oil	- Food feedstock - Competition with the edible oil market - Impact on food markets and security - Large portions of land are required
Second generation	- Jatropha oil - Sea mango - Tobacco seed oil - Tallow - Frying oil	- Low competition with food - Environmentally friendly - Poor performance in cold temperature - Animal fats (biosafety problems) - Valorization of residue

The transesterification of triglycerides with short-chain alcohols generates biodiesel and glycerol as byproducts (Figure 1), in such a way that about a 10 wt.% of glycerol, with respect to biodiesel, is produced [6]. In recent years, the worldwide production of biodiesel is growing progressively (Figure 2) [7], and glycerol production has also risen consequently, so this in-stock glycerol should have a commercial outlet to improve the sustainability of biodiesel production.

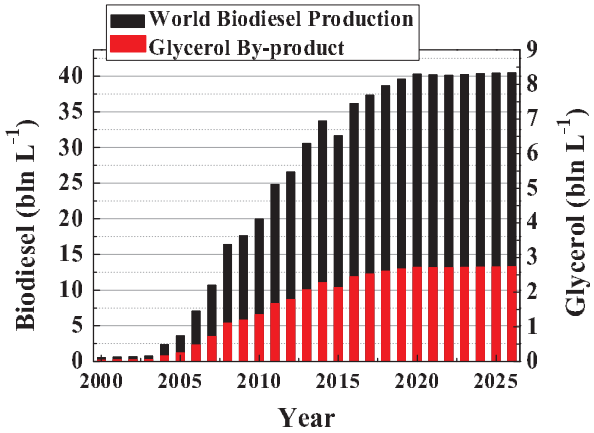

Figure 2. World production of biodiesel and glycerol (predictions of Organisation for Economic Co-Operation and Development/Food and Agriculture Organization of the United Nations (OECD-FAO)) [7].

Thus, glycerol can be transformed into value-added products. In this context, the catalytic dehydration of glycerol can yield acrolein, which is a versatile intermediate that is largely employed in the chemical industry. The presence of acid catalysts is needed to provide a suitable control of the reaction for attaining a significant acrolein yield. However, it has been demonstrated that the catalytic activity depends on the textural properties, mainly the pore size, which directly affects the deactivation processes [8–10].

The present review is included within a special issue titled "Mesoporous Silica Catalysts", and this will be focused on the use of catalysts in which the mesoporous silica plays an important role, as support of the active phase or as catalyst itself, in glycerol valorization via its transformation to acrolein.

2. Glycerol Valorization

Glycerol is an organic molecule with three hydroxyl groups, which make glycerol very soluble in polar solvents, such as water and alcohols. Moreover, the hydroxyl groups form an extensive network of hydrogen bonds, as their boiling temperature is high in relation to their molecular size. Moreover, its presence provides glycerol molecules with a high versatility and physicochemical properties, allowing direct applications for facilitating the synthesis of high value-added chemicals.

Nowadays, glycerol finds more than 1500 applications across several industries, including food, pharmaceutical, personal care, antifreeze, and vibration dampening, among others [8]. In fact, the United States Department of Energy has considered glycerol to be one of the major building block chemicals [11]. Despite its high potential, the current situation is different, since the crude glycerol obtained from triglycerides transesterification has a low quality, which is one of the reasons for the marginal price of this byproduct. For this reason, it is generally burned, thus wasting this organic raw material with a high potential for obtaining a large spectrum of valuable chemicals.

In this sense, the high glycerol reactivity allows its oxidation, partial or total hydrogenation, dehydration, and esterification or etherification, among other chemical transformations (Figure 3). In addition, glycerol can incorporate other heteroatoms, such as chorine by chlorination, or nitrogen by ammoxidation [12–14]. Among all this plethora of valorization routes, the present review will be focused on dehydration reactions.

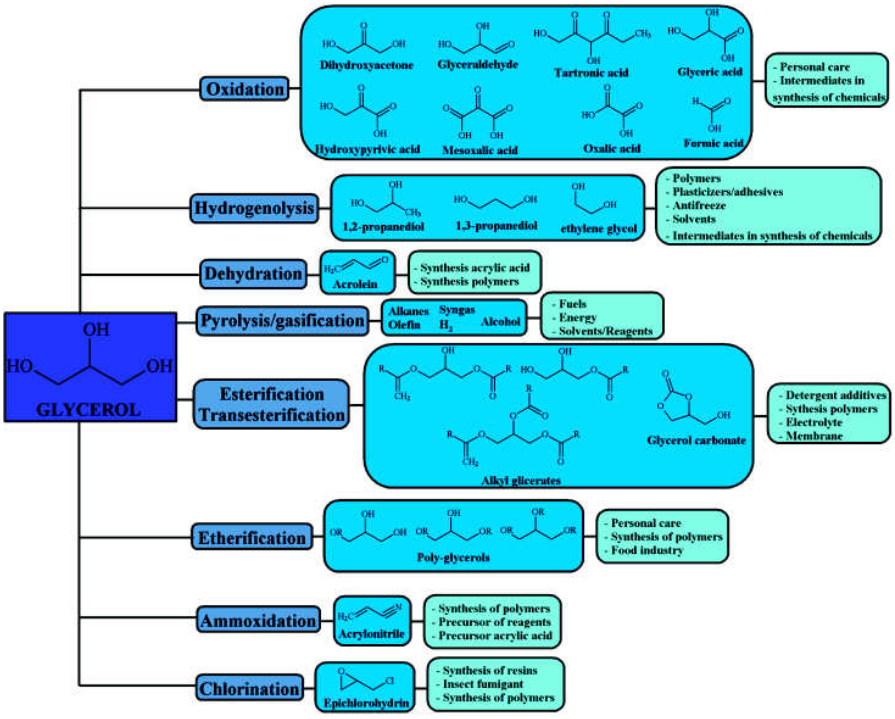

Figure 3. Valorization of glycerol and applications of some value-added products.

3. Glycerol Dehydration

One of the most interesting reactions for glycerol valorization is its dehydration to yield acrolein. This commodity is an important intermediate for the synthesis of methionine, methylpyridines, acrylic acid and esters, detergents, polymers, and super-adsorbents, and it can also be employed as biocide [8,14].

The glycerol dehydration to acrolein has been studied in both gas and liquid phases, although several authors have established that the gas phase is a more sustainable process, due to the operational and environmental issues of liquid phase reactions [15,16]. The glycerol dehydration requires acidic conditions, since the protonation of glycerol causes a decrease of the activation energy barrier from about 60 KJ mol^{-1} to 20 KJ mol^{-1} [17]. In this context, a relationship has been established between the strength of acid sites, according to the Hammett acidity, and the catalytic activity [18–20]. Thus, catalysts with the highest selectivity toward acrolein were those whose Hammett acidity was in the range $-3 < Ho < -8.2$. Several solid acid catalysts, such as metal sulfates [18,21,22] and phosphates [23–25], metal oxides (Al_2O_3, ZrO_2, TiO_2, WO_3, Nb_2O_5, Ta_2O_5), zeolites [18,26–36], and heteropolyacids [18,37–40], have shown to be active in glycerol dehydration, with a high selectivity to acrolein. Among these catalysts, metal sulfates and phosphates or heteropolyacids exhibit mainly Brönsted acidity, while others such as Al_2O_3 or ZrO_2 can be considered Lewis acid catalysts. Nevertheless, the most common is the coexistence of both Brönsted and Lewis acid sites, although it is not still clear which type of acidity is the most beneficial for glycerol dehydration.

Alhanash et al. [39] established that Brönsted acid sites favor the protonation of the secondary hydroxyl group of glycerol, which is easily dehydrated to 1,3-dihydroxypropenal and then, after a keto-enol tautomerization, it is converted to 3-hydroxypropanal, whose subsequent dehydration leads to acrolein (Figure 4).

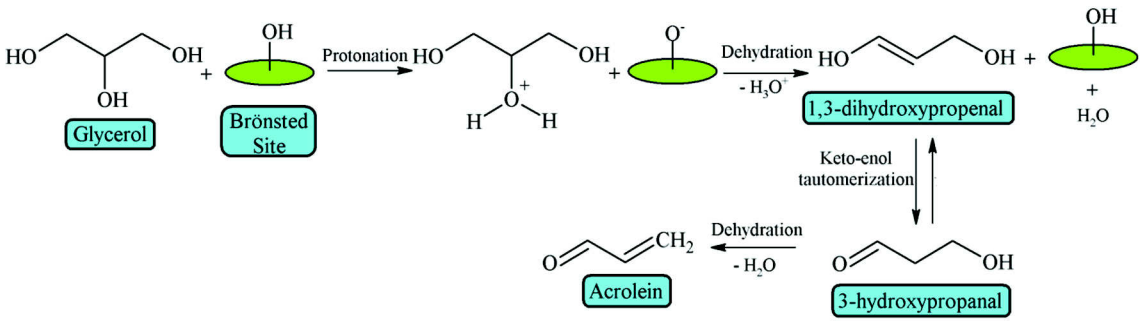

Figure 4. Mechanism of glycerol dehydration on Brönsted acid sites (adapted from Alhanash et al. [39]).

On the other hand, Lewis acid sites preferentially activate the terminal hydroxyl groups due to the steric hindrance [39] (Figure 5). The interaction between a terminal OH group and a Lewis acid site favors the H transfer from the secondary C atom to the bridging O atom of the metal oxide, giving rise to 2,3-dihydroxypropene, which tautomerizes to acetol (hydroxyacetone), and the Lewis acid site is regenerated by thermal dehydration.

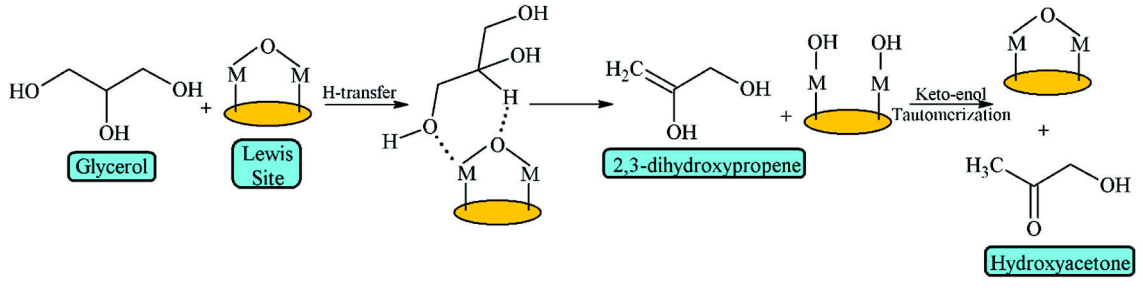

Figure 5. Mechanism of glycerol dehydration on Lewis acid sites (adapted from Alhanash et al. [39]).

It can be observed that Lewis acid sites are transformed during the formation of 2,3-dihydroxypropene into pseudo-Brönsted acid sites, which can also lead to acrolein, or be regenerated to act as Lewis acid, favoring the formation of acetol [8].

On the other hand, Laino et al., from Density Functional Theory (DFT) studies, have proposed an alternative mechanism for glycerol dehydration to acrolein [41] (Figure 6). They suggest that the reaction takes place on Brönsted acid sites, generating an epoxide (glycidol) prior to the formation of 1,3-dihydroxypropenal. Then, this aldehyde is dehydrated to form acrolein, or an intramolecular hydrogen-transfer reaction can occur, leading to formaldehyde and vinyl alcohol.

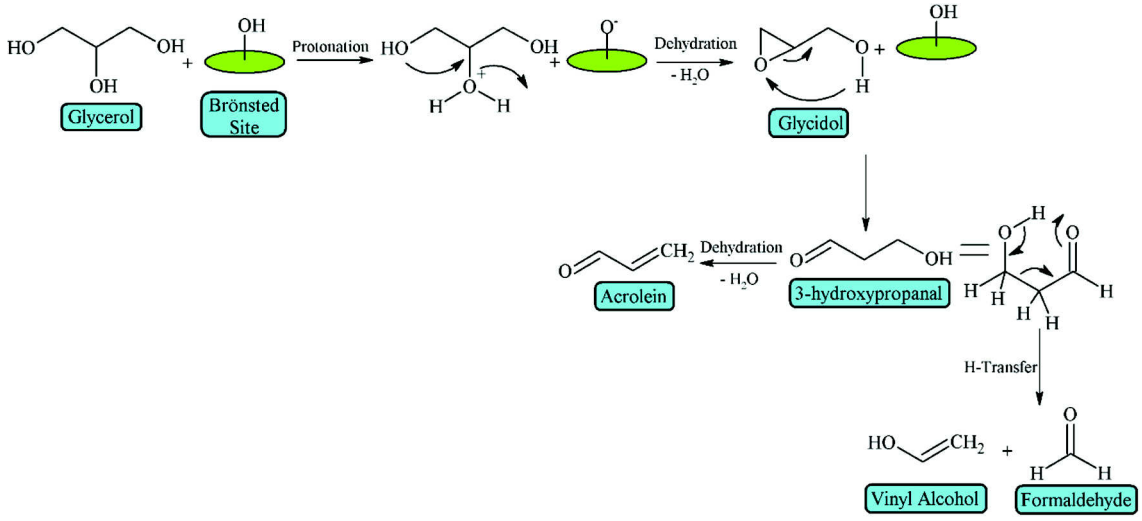

Figure 6. Alternative mechanism of glycerol dehydration on Brönsted acid sites (adapted from Laino et al. [41]).

However, it has been reported that other factors influence the catalytic performance besides the catalyst acidity, such as its textural properties. Thus, Tsukuda et al. [9] evaluated different supported heteropolyacids as catalysts for glycerol dehydration to acrolein, demonstrating that the catalytic activity depended on the type of heteropolyacid and on the size of mesopores of the silica support. They reported that silicotungstic acid supported on silica with mesopores of 10 nm exhibited a stable catalytic activity, obtaining a C_{gly} (glycerol conversion) = 100% and Y_{acrol} (Acrolein Yield) = 86%) in such a way that the size of the mesopores affected the catalytic activity, since small mesopores of 3 nm induced deactivation (C_{gly} = 55% and Y_{acrol} = 36%). Likewise, Pathak et al. [10] studied Zeolite Socony Mobil-5 (ZSM-5) zeolites with different pore sizes (0.54 nm, 0.74 nm, 3.15 nm, and 11.2 nm) and detected that the acrolein selectivity enhanced with the pore size, although selectivity toward other byproducts, such as formaldehyde, acetaldehyde, or hydroxyacetone, also increased. Therefore, the presence of mesopores seems to be directly related to the catalytic activity.

4. Mesoporous Silica-Based Catalysts Used in the Glycerol Dehydration

In this section, the most relevant silica-based catalytic systems studied for glycerol dehydration will be reviewed, in particular those employing a mesoporous silica as support or catalyst.

4.1. Mesoporous Silica

Since the Mobil company (Irving, TX, Estados Unidos) discovered the M41S family of mesoporous materials in 1992, much attention has been paid to mesoporous silica due to its use as catalyst in the oil refining and petrochemical industry or its use as adsorbent in separation processes. The synthesis of these mesoporous solids is based on the use of cationic surfactants as structure-directing agents (SDA) for the formation of the hybrid organo-inorganic precursor, which after subsequent calcination, or

surfactant extraction, gives rise to a mesoporous framework. The formation of micellar structures helps build up the siliceous framework by polymerization of the silica precursors. This methodology allows the synthesis of mesoporous solids with a narrow pore size distribution, ranging between 2–6.5 nm [42]. Later, Stucky et al. at the University of Santa Barbara synthesized a new ordered mesoporous silica, using triblock copolymers as SDA, originating materials with pore diameters between 5–30 nm [43]. Their high specific surface area together with a narrow pore size distribution favored the dispersion of active phases and the diffusion of molecules. The use of these mesoporous materials in glycerol dehydration is compiled in Table 2.

On the other hand, the presence of silanol groups (–Si–OH) on the silica walls allows the surface functionalization of the mesoporous silica by grafting. Thus, several authors functionalized the SBA-15 mesochannels by the grafting of mercaptopropyl trimethoxysilane. The –SH groups were then oxidized with H_2O_2 to generate sulfonic groups (SO_3H) (Figure 7). These catalysts were active in the dehydration of glycerol due to the presence of Brönsted-type acidity on the surface of the mesoporous silica [44,45].

Table 2. Catalytic activity of catalysts based on mesoporous silica in glycerol dehydration.

Active Phase	T (°C)	TOS (h)	C_{gly} (%)	Y_{acrol} (%)	$Mmol_{acrol}\ h^{-1}\ g_{cat}{}^{-1}$	Ref.
SBA-15-SO_3H	300	3	100	93	10.5	[44]
SBA-15-SO_3H	300	6	45	35	13.9	[45]
SBA-15-PO_3H	320	2	97	81	3.71	[46]
Meso SiO_2-ZrO_2/$SO_4{}^{2-}$	250	2	99	81	10.9	[47]
$H_3PW_{12}O_{40}$/MCM-41	320	2	85	68	3.72	[48]
$H_3PW_{12}O_{40}$/MCM-41	320	5	87	44	3.59	[49]
$H_6P_2W_{18}O_{62}$/MCM-41	320	5	82	51	4.20	
$Cs_{2.5}H_{0.5}PW_{12}O_{40}$/MCM-41	300	2	100	86	8.47	[50]
$Cs_{2.5}H_{0.5}PW_{12}O_{40}$/MCM-41	300	30	100	88	24.08	[51]
MCM41-Zr	320	5	74	19	0.87	
Pd-HPW/Zr-MCM-41	320	5	94	80	3.64	[52]
Pt-HPW/Zr-MCM-41	320	5	83	62	2.82	
MCM41-Zr	300	5	66	18	5.31	[53]
Pt-HPW/Zr-MCM-41	350	5	82	70	20.31	
$H_4PMo_{11}VO_{40}$/SBA-15	225	4	100	74	1.69	[54]
MCM41-Zr	315	5	97	38	5.28	[55]
MCM41-Zr	250	0–5	96	71	4.86	[56]
V_2O_5/MCM41-Zr	325	2	90	25	4.41	[57]
V_2O_5-P/MCM41-Zr	325	2	90	41	6.71	
Nb_2O_5/MCM-41-Zr	325	2	77	45	7.43	[58]
WO_3/MCM-41-Zr	325	2	97	41	6.71	[59]
WO_3-P/MCM-41-Zr	325	2	78	51	8.36	
Nb_2O_5-P/MCM-41-Zr	325	2	100	56	9.18	[60]
Al-SBA-15	325	2	94	35	5.74	[61]

TOS (Time On Stream). C_{gly} (Glycerol Conversion). Y_{acrol} (Acrolein Yield).

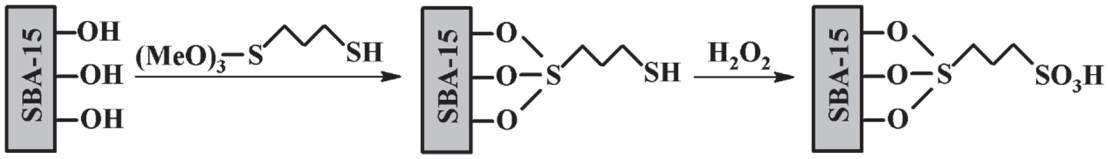

Figure 7. Functionalization of silica with sulfonic groups.

Lourenço et al. found that sulfonic acid groups incorporated to SBA-15 by the addition of 3-mercaptopropyltrimethoxysilane, which achieved a high acrolein yield (93%) and minimized the catalyst deactivation (Table 2). In addition, the large pore size of open channels of the SBA-15 silica favored the mass transfer and prevented deactivation [44]. These authors affirmed that both the pore

size and density of acid sites played an important role in the deactivation rate and selectivity pattern, since a larger pore size significantly improved the catalytic activity, whereas a high density of acid sites could reduce acrolein production. However, Dalla Costa et al. observed a progressive deactivation under more severe reaction conditions (Table 2) [45]. They found that higher temperatures led to rapid deactivation due to a combined effect associated with coke deposition and the decomposition of sulfonic acid groups. Thus, temperatures above 300 °C provoked an irreversible deactivation. In both cases, the sulfonic acid groups were highly selective toward acrolein, with hydroxyacetone being a minor product and the density of sulfonic groups directly related to the catalytic activity.

Another strategy to generate Brönsted acid sites on the surface of mesoporous MCM-41 silica was by impregnation with phosphoric acid and subsequent calcination [46]. This catalyst followed the same trend as that observed for the mesoporous silica functionalized with sulfonic acid groups, since the main product was acrolein (Table 2) with a negligible amount of hydroxyacetone. This catalyst maintained the glycerol conversion (97%) during 10 h, but deactivation by coke deposition was detected for a longer reaction time, which was more pronounced than that observed for SBA-15 silica due to the narrower pore size of MCM-41, which favors a faster pore blockage. However, the H_3PO_4-modified MCM-41 catalyst recovered its activity after regeneration by a simple oxidative treatment in air.

Kobayashi et al. studied a mesoporous sulfated zirconia/silica catalyst with 20 wt.% SO_4^{2-} in the catalyst, which was incorporated by using $(NH_4)_2SO_4$ solutions [47]. They observed that sulfate groups provided Brönsted acid sites, although the most active and stable catalyst was that with a lower proportion of Brönsted acid sites, since its higher surface area minimized the formation of carbonaceous deposits. They proposed the existence of weak acid sites due to the dilution of zirconium species into silica, whereas the large pore size is suitable for a faster diffusion of glycerol, giving rise to better catalytic performance. The catalyst deactivation took place without the loss of sulfur, being ascribed to the covering of acid sites by coke.

The use of mesoporous silica also allows hosting and dispersing bulky polyoxocations, such as heteropolyacids, which enhance the acidity strength, especially of Brönsted acid sites. Thus, Ding et al. incorporated different loadings of $H_3PW_{12}O_{40}$ into MCM-41 by impregnation, maintaining within the resulting solids a high specific surface area, determined by the Brunauer, Emmett and Teller (BET) equation, S_{BET} (415–624 m^2 g^{-1}) and pore size values (2.5–2.7 nm). The highest catalytic activity (C_{gly} = 85% and Y_{acrol} = 65%) (Table 2) was found for the catalyst with a 40 wt.% of $H_3PW_{12}O_{40}$ [48]. Alike, Ma et al. compared two phosphotungstic acids ($H_6P_2W_{18}O_{62}$ and $H_3PW_{12}O_{40}$) supported on MCM-41 by using the wet impregnation method [49]. They established from pyridine adsorption coupled to Fourier transform infrared (FT-IR) spectroscopy that a $H_3PW_{12}O_{40}$/MCM-41 catalyst showed a higher total acidity, mainly of Lewis type, while $H_6P_2W_{18}O_{62}$/MCM-41 displayed the highest Brönsted:Lewis acid sites ratio. These data could be correlated with the catalytic behavior, since $H_6P_2W_{18}O_{62}$/MCM-41, with a higher proportion of Brönsted acid centers, was more selective toward acrolein (Table 2). On the other hand, the presence of a higher fraction of Lewis acid sites in $H_3PW_{12}O_{40}$/MCM-41 catalyst caused a decrease in the acrolein selectivity, with a concomitant increase in hydroxyacetone. They also confirmed that catalyst deactivation was caused by both the leaching of HPW species and coke deposition.

One of the main drawbacks related to the use of heteropolyacids supported on mesoporous silica is related to their deactivation. Due to the high catalytic activity of this phase, leading to high acrolein yields, carbonaceous deposits are easily generated that block mesochannels, which gives rise to a faster deactivation associated with diffusional limitations. In this regard, several authors have proposed that the incorporation of Cs^+ species into heteropolyacids supported on mesoporous silica can minimize the deactivation by coke deposition, since Cs^+ partially neutralizes the strongest acid sites of heteropolyacids (Table 2) [50,51]. Other cations, such as Na^+ or K^+, were also proposed in order to reduce the formation of carbonaceous deposits; however, these cations drastically decrease the number of strong acid centers, which led to a lower catalytic activity and yield toward acrolein [51].

The deactivation also minimized incorporating O_2 in the gas carrier, although the oxygen concentration had to be limited, since carbonaceous deposits could burn [50].

Other authors pointed out that the doping of heteropolyacids supported on mesoporous silica with noble metals, such as Pd or Pt, could reduce the coke, thus ameliorating the catalytic performance (Table 2) [52,53]. Trakarnpurk confirmed that the presence of platinum improved the long-term stability of a ZrMCM-41 impregnated with 2% Pt and 35% phosphotungstic acid catalyst [53]. The Pt-free catalyst exhibited an abrupt decrease in conversion (until 60% after 20 h of time-on-stream) due to coke deposition. In the same way, Ma et al. [52] demonstrated that a Pd-$H_3PW_{12}O_{40}$/Zr-MCM-41 catalyst, prepared by impregnation, significantly enhanced the acrolein selectivity, with lower coke deposition and improved stability, with the support mesostructure remaining almost unchanged.

On the other hand, Viswanadham et al. established that the incorporation of vanadium species in the heteropolyacid structure also minimized the coke deposition, due to the redox properties of vanadium species retarding the deactivation [54]. These authors also observed a faster deactivation for the heteropolyacid supported in porous materials with a narrower pore diameter (Y-zeolite), while the use of large pore supports, such as SBA-15, maintained the catalytic activity for longer reaction times, because larger channels can avoid the pore blockage. However, the pore size distribution must be tuned to ensure an appropriate interaction between glycerol and the active centers.

The incorporation of heteroatoms, such as zirconium (IV) or aluminum (III), into a mesoporous silica is a classical methodological approach to generate acid sites for glycerol dehydration. Thus, the substitution of an Si (IV) atom by a heteroatom increases the acid strength of Si–OH groups, whereas the formation of M–OH–Si linkages, similarly to Si–OH–Al groups in zeolites, creates new Brönsted acid sites [55,62,63]. In this process, Lewis acid sites can be also formed, which are associated with deficiently coordinated heteroatoms. However, these Lewis acid centers can be transformed into pseudo-Brönsted sites by the water present in the reaction medium, as previously reported [8]. García-Sancho et al. synthesized a zirconium-doped mesoporous MCM-41 silica, incorporating Zr species into the siliceous framework, with different Si/Zr molar ratios (4–12), obtaining a maximum glycerol conversion of 97% with an acrolein yield of 39% after 2 h of time-on-stream at 325 °C for a Si/Zr molar ratio of five (Table 2) [55]. They also detected a high proportion of acetaldehyde, which can be formed by the retro-aldol fragmentation of 3-hydroxypropanal at reaction temperatures above 300 °C [52]. However, other authors established that acetaldehyde could result from the decomposition of hydroxyacetone [64]. Unfortunately, Zr-MCM-41 catalysts showed a rapid deactivation. Moreover, heteroatom-doped mesoporous silica has been used as a support of heteropolyacids. This work aims to weaken the strength of the Brönsted acid sites being associated with heteropolyacids by their interaction with the support. Consequently, the formation of carbonaceous deposits was reduced, leading to more stable catalysts [52,56]. It was also observed that the presence of zirconium into the siliceous framework favored the catalyst regeneration in comparison to the catalyst without zirconium [65].

Different metal oxides, such as V_2O_5 [57], Nb_2O_5 [58], and WO_3 [59], have been incorporated into a mesoporous silica doped with zirconium by incipient wetness impregnation using vanadyl acetylacetonate, niobium oxalate, and ammonium metatungstate hydrate as precursor salts, respectively, causing an increase in both Lewis and Brönsted acidity, due to the interaction of zirconium species with metal oxides. Brönsted and Lewis acid sites, which are transformed into pseudo-Brönsted acid sites, favored acrolein formation and reduced their deactivation by coke. In all of the cases, the thermal decomposition of acrolein led to acetaldehyde as byproduct. It can be observed in Table 2 that supported Nb_2O_5 species were more selective to acrolein than V_2O_5 and WO_3. Later, phosphorus species were incorporated to these metal oxides, obtaining an amorphous pseudo-heteropolyacid after calcination [57,59,60]. The incorporation of high phosphorus contents by using phosphoric acid solutions caused a pore blockage, so the catalytic processes in these cases could take place mainly on the external surface. In spite of the decay of the specific surface area, the density of acid sites increased, as well as the proportion of Brönsted acid sites, leading to a higher acrolein yield and a decrease in

carbon deposits. Therefore, these catalysts were more stable along the time-on-stream, even if only active sites located on the external surface were involved in the catalytic process.

On the other hand, Cecilia et al. employed a low-cost SBA-15 synthesized from sodium silicate, and carried out a partial extraction of the silicon species from the siliceous framework using basic conditions [61]. Later, aluminum species were incorporated into the siliceous framework by mixing different volumes of a 1.2 M $AlCl_3 \cdot 6H_2O$ aqueous solution with 25 mL of tetramethylammonium hydroxide aqueous solution. The existence of two kinds of aluminum sites was inferred from ^{27}Al-NMR spectroscopy: tetrahedral Al located inside the silica walls and extra-framework octahedral Al species. Pyridine adsorption studies indicated that the tetrahedral aluminum generated Brönsted acid sites, while the presence of octahedral aluminum, whose amount rose with the Al loading, caused an increment of total acidity and the amount of Lewis acid sites, but the concentration of Brönsted acid sites decreased. Therefore, a higher proportion of aluminum did not produce an increase in tetrahedral aluminum, since firstly, the aluminum was introduced into the framework defects, and the excess remained on the external surface of SBA-15 as octahedral aluminum, which displayed a lower catalytic activity in glycerol dehydration to acrolein. Although the acrolein yield was lower than that obtained for other catalysts (Table 2) and the active sites suffered deactivation by coke deposition, this Al-SBA-15 catalyst could be interesting, since it is a simple and inexpensive catalyst and it could be reused, at least during three catalytic cycles after thermal regeneration.

4.2. Zeolites

Zeolites have demonstrated to be highly active in glycerol dehydration to acrolein, due to the existence of strong Brönsted acid centers in the microporous structure. The catalytic data reveal that the SiO_2/Al_2O_3 ratio is not the only factor influencing glycerol conversion and the selectivity pattern, but there must be other factors involved in the catalytic performance, such as the type of zeolitic framework or the pore dimensions and topology [32,34,66]. In general, the catalytic activity was directly related to the amount and strength of Brönsted acid sites, although the dimensions of cavities played a key role in determining the resistance to deactivation [34,67–69]. As the current review is only focused on mesoporous silica catalysts, microporous zeolites used in glycerol dehydration will not be dealt with.

Kim et al. [34] compared the catalytic performance of H-β, H-ferrierite, H-ZSM-5, H-Y, and H-mordenite with different SiO_2/Al_2O_3 molar ratios (SiO_2/Al_2O_3 = 5.1–350). The glycerol conversion was strongly dependent on their external surface area. However, most of the pores, mainly micropores, were filled with carbonaceous species at the initial stage of this reaction, provoking the catalyst deactivation. Carriço et al. employed a MCM-22 with different SiO_2/Al_2O_3 molar ratios (30–80) prepared by using silica and aluminum nitrate as solid acid catalyst [66], and concluded that its crystallinity, as well as its textural properties, worsen for higher SiO_2/Al_2O_3 molar ratios. Although MCM-22 catalysts were essentially microporous, the presence of secondary mesopores was detected. However, they found that an increase in the SiO_2/Al_2O_3 molar ratio was accompanied by a reduction of the external surface area and a decrease of the mesoporous volume. The catalytic data showed that the catalyst with the highest acidity was that with the lowest SiO_2/Al_2O_3 molar ratio, reaching the best acrolein yield.

Therefore, the coke deposition is directly related to the porous structure. Thus, zeolites with narrower pores are more susceptible to suffer pore blockage, and consequently they are deactivated more quickly. However, zeolites with larger pore volume, or open channels, are more resistant to blockage after short reaction times, since the diffusion is favored. Rodrigues et al. confirmed, by analyzing the carbonaceous deposits by ^{13}C-NMR, the existence of aromatic and polyglycol deposits (Figure 8A–C) [68,70]. They concluded that polyaromatic species are formed inside pores on highly active Brönsted acid centers (Figure 8D_1), in the first hours of reaction, whereas polyglycol deposits took place on the external surface of zeolites, since glycerol molecules were not able to access to the zeolitic cavities (Figure 8D_2).

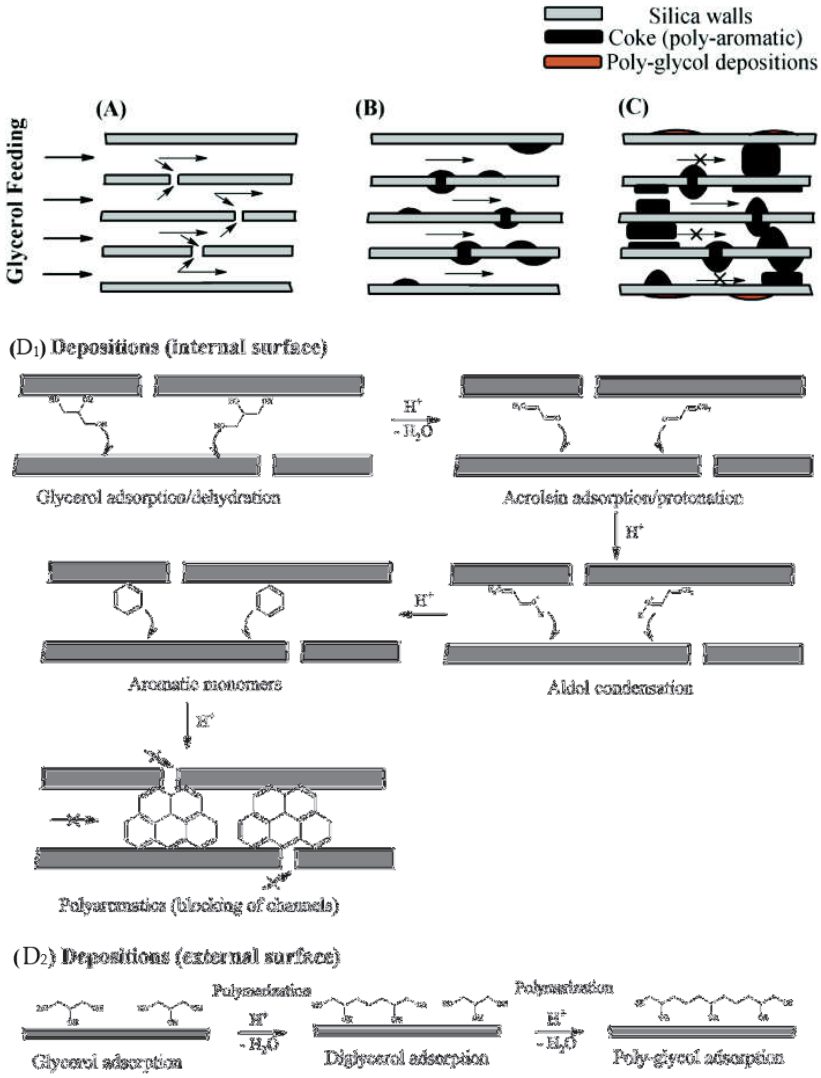

Figure 8. Scheme of the formation of carbonaceous deposits (**A**–**C**). Deposits formed on the internal surface (**D1**) and deposits formed on the external surface (**D2**).

In order to obtain more stable catalysts along the time-on-stream, the generation of mesoporosity by partial structural desilication, under basic conditions, has been proposed. Under these alkaline conditions, by using NaOH solutions, the SiO_2/Al_2O_3 molar ratio should decrease, leading to a higher amount of available acid sites [71]. However, the desilication also caused the extraction of aluminum, which generated Lewis acid sites, so the selectivity to hydroxyacetone may increase. The catalyst stability was improved upon desilication due to an increase in coke tolerance. In addition, NH_3-thermoprogrammed desorption (NH_3-TPD) studies revealed a decrease of surface acidity strength, so the desilication had an antagonist effect [72]. Nonetheless, other authors pointed out that the Lewis acidity has a cooperative role with neighboring Brönsted centers, improving the catalytic activity [73]. In order to remove the extra-framework alumina associated with Lewis acidity, Lari et al. carried out a subsequent acid treatment to dissolve the aluminum debris, producing an improvement in the selectivity toward acrolein [74].

The coke deactivation can also be slowed down by synthesizing hierarchical zeolites with lower channel lengths. Thus, Zhang et al. evaluated the influence of the mesoporosity and acidity of hierarchical H-ZSM-5 zeolites on the catalytic performance, obtaining a higher coke resistance for the H-ZSM-5 with abundant open inter-crystalline mesopores, maintaining a full glycerol conversion after 14 h of time-on-stream (TOS) [75]. On the contrary, H-ZSM-5 catalysts with closed intercrystalline pores start

to deactivate after 6 h of TOS [75]. Therefore, these results confirmed that an open and interconnected mesoporous architecture leads to a high activity, long lifetime, and improved selectivity, while the worse behavior of closed and small mesopores was attributed to the mass transfer limitations and/or the in-pore condensation of reactant or heavier reaction products. They also emphasized the need to design zeolites with proper hierarchical structure and acidity for maximal catalytic performance.

In the same way, Beerthuis et al. compared a commercial H-ZSM-5 with a hierarchical H-ZSM-5, micro-H-ZSM-5, and nano-H-ZSM-5 [76], being the catalytic results directly related to textural parameters. In this sense, the hierarchical H-ZSM-5 zeolite, with a higher pore volume and lower microporosity, reached the highest glycerol conversion and selectivity to acrolein, while the micro-H-ZSM-5, formed by microsized crystals with small micropores, suffered a faster deactivation by pore blocking. They related the improved stability and coking resistance to the hierarchical porosity formed by micropores, mesopores, and macropores. A similar result was reported by Huang et al., which synthesized a hierarchical H-ZSM-5 by an ultrasound-assisted method, obtaining a catalyst with longer life than the commercial catalyst [77].

Dos Santos et al. prepared ferrierite zeolites in fluoride medium as a mineralizing agent, which resulted in the formation of large crystals [78]. These authors compared the textural properties and catalytic behavior with that of a ferrierite synthesized by the classical method using a hydroxide medium. They found that the ferrierite zeolite synthesized in fluoride medium displayed a lower density of acid sites, which was probably due to the existence of Al–F bonds instead of Al–OH bonds; however, this catalyst was more active and stable than the traditional ferrierite.

Viswanadham et al. generated a high amount of Brönsted acid sites into a Y-zeolite by incorporating 10–40 wt.% of $H_3PW_{12}O_{40}$ using a wetness impregnation method [79]. They attained the highest acrolein yield (79%) after 3 h of TOS at 275 °C for the catalyst with a 20 wt.% of $H_3PW_{12}O_{40}$. However, the use of a higher loading of heteropolyacids did not improve the activity and/or the stability of the catalyst, which was explained by the partial collapse of the zeolite structure, as deduced from textural characterization. Thus, the acrolein selectivity decreased for higher phosphotungstic acid loadings due to the diffusional limitations associated with the smaller pore size.

Again, the incorporation of a low amount of noble metals helped to minimize the coke formation, delaying the catalyst deactivation. These noble metals can be catalytically active, giving rise to other high value-added products. In this sense, Lari et al. synthesized bifunctional catalysts based on noble metals (Ag, Au, Pd, Pt, and Ru) with a 5 wt.% metal loading supported on a Mordenite Framework Inverted (MFI) type zeolite treated under basic conditions with NaOH aqueous solutions to increase the dimensions of cavities [74]. They pointed out that the alkaline treatment generates an auxiliary network of intracrystalline mesopores, thus increasing the coking resistance and providing a longer lifetime in glycerol dehydration. The catalytic results revealed that the zeolite catalyzed the dehydration of glycerol to acrolein, while the noble metal acted as hydrogenation sites for acrolein, obtaining the highest allyl alcohol selectivity for the Ag-based catalyst and the highest propanal selectivity for the Pd-based and Pt-based catalysts.

The incorporation of vanadium species in zeolites also exerts a beneficial effect on dehydration reactions due to the redox properties associated with vanadium, slowing the deactivation by coke. Moreover, the use of O_2 as co-feed retarded the deactivation process and also favored the oxidation reaction of acrolein to acrylic acid in a process called oxidehydration (Figure 9). Acrylic acid is a valuable compound that is used in the manufacture of plastics, coatings, adhesives, and elastomers, as well as floor polishes and paints.

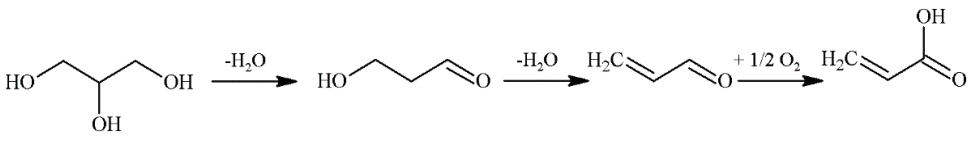

Figure 9. Reaction of glycerol oxidehydration to acrylic acid.

In a detailed study, several zeolites with different textural properties were impregnated with vanadium (5 wt.%) by using NH_4VO_3 solutions [80]. The use of N_2/O_2 as the carrier gas led to a negligible deactivation, except for those catalysts with a higher microporosity, or a higher SiO_2/Al_2O_3 molar ratio, which suffered a slight deactivation after 10 h of TOS. In all of the cases, strong Brönsted acid sites associated with the zeolite framework were responsible for glycerol conversion to acrolein, whereas vanadium species oxidized by a Mars–van Krevelen cycle using mobile lattice oxygen, where V^{5+} was partially reduced to V^{4+} [70]. With regard to the selectivity, in all of the cases, acrolein was the main product, reaching yields between 12.7–46.8%, while acrylic acid was a minority product, obtaining a yield of 17.7% for V-β zeolite in the best case. These data followed the same trend as that shown for Pestana et al. for the same catalyst under milder reaction conditions [81], and also were in agreement with data obtained for V/MFI (SiO_2/Al_2O_3 = 40) catalysts [70].

4.3. Silicon-Aluminophosphate (SAPO)

Aluminophosphates ($AlPO_4$-n, where n denotes a structure type) were described by Wilson et al. in 1982 as a new class of zeolite-like molecular sieves [82]. These microporous materials are built up from a trick alternation of AlO_4 and PO_4 tetrahedra through corner sharing to form a neutral open framework. The neutrality of the $AlPO_4$ structure limits its catalytic applications in dehydration reactions due to the absence of Brönsted acid sites. However, the substitution of phosphorus by silicon in the framework modifies the physicochemical properties, generating Brönsted acid sites [83], which are necessary for glycerol dehydration.

Several SAPOs (SAPO-11, SAPO-34, and SAPO-40) were evaluated in glycerol dehydration [84]. The catalytic results revealed a significant deactivation along the time-of-stream, being more pronounced in the case of SAPO-11 and SAPO-34 (Table 3). Lourenço et al. also indicated that the deactivation was directly related to the porous structure. The deactivation of SAPO-34 was more abrupt than that of SAPO-40 in spite of their similar microporous volume, due to the cage openings of SAPO-34 being much smaller than the pores of SAPO-40, leading to pore blocking by coke formation. In any case, the acrolein yield was higher than that previously reported by Chai et al. for SAPO-34 at short reaction times [18]. In the case of SAPO-11, an intermediate behavior was observed, since pore architecture influenced both the catalytic performance and the deactivation. Therefore, it seems clear that the porous network of solid acid catalysts had a strong influence on glycerol dehydration. Thus, for instance, SAPO-40, with a more open structure and a higher S_{BET} value, proved to be highly resistant under the experimental conditions used, and it was regenerated without a loss of activity or significant structural damages.

Table 3. Catalytic activity of SAPO-11, SAPO-34, and SAPO-40 in glycerol dehydration.

Catalyst	T (°C)	TOS (h)	C_{gly} (%)	Y_{acrol} (%)	$Mmol_{acrol}\ h^{-1}\ g_{cat}^{-1}$	Ref.
SAPO-11	350	2.5	100	73	2.4	[84]
		120	26	19	0.6	
SAPO-34	350	2.5	90	69	2.3	
		120	16	12	0.4	
SAPO-40	350	2.5	100	75	2.5	
		120	54	39	4.0	
SAPO-34	315	9	32	15	0.1	[18]
SAPO-11	280	1	88	55	0.9	[25]
SAPO-34	280	1	59	42	0.7	
Meso-SAPO-40	320	2.5	100	81	2.7	[85]
	320	120	87	68	2.3	

Regarding the selectivity, SAPOs showed similar acrolein selectivity, about 75%, and the presence of hydroxyacetone and acetaldehyde was also noteworthy (about 10% of selectivity) [84]. These data are in disagreement with those reported by Suprun et al., where the hydroxyacetone selectivity was higher [25]. They reported that SAPO-11 and SAPO-34 catalysts, with small micropores (5–6 Å), were less active but more selective than mesoporous Al_2O_3–PO_4 and TiO_2–PO4. Moreover, a detailed study with SAPO-40 revealed that the use of high reaction temperatures (T > 350 °C) causes a drastic deactivation by the formation of carbonaceous deposits, although the catalyst can be easily regenerated, maintaining its catalytic performance [84,85].

Recently, Fernandes et al. synthesized a mesoporous SAPO-40, using an organosilane as an additional porogen agent, replacing part of the silica source (Cab-OSil-M5) in the synthesis gel by [3-(trimethoxysilyl)propyl]-octadecyldimethyl-ammonium chloride, increasing the external surface area and mesopore volume [85]. In comparison to traditional SAPO-40, the long-term stability of mesoporous SAPO-40 is notably higher, demonstrating the beneficial effect of mesoporosity. Thus, an increase in the pore volume diminishes the diffusional limitations caused by the blockage of the structure with carbonaceous deposits and facilitates the access to acid sites.

4.4. Commercial Silica

Generally, commercial silica displays a spherical morphology with high porosity, with a high specific surface area associated with interparticle voids. In spite of this porosity, the weak acidity of the silica is not enough to favor the glycerol dehydration to acrolein. Thus, SiO_2 is usually employed as support or mixed with active oxides to disperse them instead of the active catalyst itself.

The morphology of the silica can be easily modulated in comparison to other oxides, which is an important parameter for attaining a suitable catalytic performance. Thus, Tsukuda et al. used a silica composed of spheres of 6 nm as support for several Keggin-type heteropolyacids (HPAs) (Table 4) [9]. These authors reported that all of the catalysts, except the catalyst with boric acid (H_3BO_3) provided high values of glycerol conversion, although the acrolein yield differed between them. Generally, the main product was acrolein, although acetaldehyde and hydroxyacetone were also detected. Moreover, it is noteworthy that the silica impregnated with phosphomolybdic acid (Q6-PMo-30) reached lower acrolein yield values because of molybdenum triggers oxidation/reduction reactions, causing the formation of other products such as acetaldehyde. In all of the cases, the activity of the HPAs was higher in comparison to SiO_2/Al_2O_3 and H_3PO_4/SiO_2 due to the presence of stronger Brönsted acid sites associated with HPAs [86]. The highest catalytic activity in glycerol dehydration was found for the silica impregnated with silicotungstic acid, and it was ascribed to both the higher thermal stability (500 °C) of this HPA and its strongest acidity in comparison to other HPAs [87].

In addition, Tsukuda chose this most active phase, the silicotungstic acid, to be supported in three silicas with different pore diameter (3 nm, 6 nm, and 10 nm) [9]. The catalytic results revealed that the silica with a lower pore diameter was more susceptible to undergo deactivation at shorter reaction times in comparison to the silica with a pore diameter of 10 nm. Therefore, they confirmed that the catalytic activity depended on both the nature of the heteropolyacid and the size of the mesopores of the silica support.

Considering the high activity of the silicotungstic acid ($H_4SiW_{12}O_{40}$), Kim et al. supported it on SiO_2-Al_2O_3, but with a low percentage of Al ($Si_{0.9}Al_{0.1}O_x$) [88]. The highest acrolein yield was 54% after 2 h of TOS (Table 4). In this sense, it has been previously established that at low Al loadings, the aluminum can be incorporated into the silica framework under basic conditions [61], exhibiting physicochemical properties similar to those of zeolites, although lacking the microporous ordering. This fact was confirmed by NH_3-TPD, which revealed that the acidity was directly related to the catalytic behavior. Therefore, the presence of HSiW in supported catalysts increased the acidity, thus providing higher catalytic activities than those of the corresponding supports. Both glycerol conversion and acrolein yield significantly decreased with increasing time-on-stream due to carbonaceous species being deposited on the strong surface acid sites, provoking a loss of accessible

active sites and decreasing the BET surface area and pore diameter, which complicated the diffusion of products.

Table 4. Catalytic activity of commercial silica-based catalysts for the glycerol dehydration reaction.

Active Phase	T (°C)	TOS (h)	C_{gly} (%)	Y_{acrol} (%)	$Mmol_{acrol}\ h^{-1}\ g_{cat}^{-1}$	Ref.
SiO_2-H_3PO_4	325	5	70	38	2.0	
SiO_2-H_3BO_3	325	5	15	0.3	0.02	
SiO_2-PW	325	5	100	65	3.9	[9]
SiO_2-PMo	325	5	98	33	2.0	
SiO_2-SiW	325	5	100	74	4.4	
SiO_2-SiW	315	2	23	6	13.1	
$Si_{0.9}Al_{0.1}O_x$-SiW	315	2	97	54	127.3	[88]
Al_2O_3-SiW	315	2	87	33	26.1	
SiO_2-PW	275	10	16	4	78.3	
$Si_{0.85}Al_{0.15}O_x$-PW	275	10	43	20	83.6	[40]
Al_2O_3-PW	275	10	13	3	13.0	
$Si_{i0.8}Al_{0.2}O_x$	315	2	43	21	50.7	[89]
SiO_2-PW	315	10	20	11	3.3	[90]
ZrO_2-PW	315	10	70	49	8.1	
$0.5Nb_2O_50.5WO_3/SiO_2$	305	1	99	47	0.4	[30]
$SiO_2/WO_3/ZrO_2$	300	8	100	65	0.5	[64]

Kang et al. carried out an analogous study using phosphotungstic acid ($H_3PW_{12}O_{40}$) supported on SiO_2-Al_2O_3, obtaining similar results [40]. These authors pointed out that the incorporation of small amounts of Al increased the proportion of Brönsted acid sites, while the progressive addition of Al-species caused an increase of the Lewis acidity, which is not beneficial for the dehydration of glycerol to acrolein. In all of the cases, the mesoporous structure of supports was maintained after the incorporation of $H_3PW_{12}O_{40}$.

Likewise, Kim et al. prepared SiO_2-Al_2O_3 catalysts by the incorporation of Al^{3+} in basic medium [89], as was previously indicated for HPAs [40,88]. These authors also observed that a small amount of Al^{3+} could be incorporated into the silica structure generating Brönsted acid sites, which favored glycerol dehydration, whereas the Lewis acidity was associated with the extra-framework Al^{3+}. Nonetheless, these values were below those obtained with HPAs under similar catalytic conditions [59], due to the HPAs displaying stronger Brönsted acid sites, which improved the catalytic performance in the dehydration of glycerol to acrolein.

In another study, Chai et al. also supported phosphotungstic acid on a commercial SiO_2 and compared its catalytic behavior to HPW/ZrO_2 catalysts [90]. Despite the textural and acidic properties of HPW/SiO_2, the catalytic data showed that the acrolein yield was higher when ZrO_2 was employed due to the stronger interaction between the ZrO_2 and the Keggin anion (Table 4).

On the other hand, the silica can be mixed with other metal oxides with greater acid strength in order to increase the amount of available sites for glycerol dehydration. Massa et al. synthesized WO_3-Nb_2O_5 supported on several oxides (SiO_2, TiO_2 and Al_2O_3). However, the catalytic data showed that those catalysts supported on SiO_2 reached the lowest acrolein yields (47% for $0.5WO_3$-$0.5Nb_2O_5/SiO_2$ catalyst) (Table 4), probably because SiO_2 is the support with the weakest acidity [30]. In all of the cases, acrolein and hydroxyacetone were obtained by the coexistence of Brönsted and Lewis acid sites; however, the main product was acrolein due to the transformation of the Lewis acid sites into pseudo-Brönsted acid sites by the presence of H_2O in the reaction medium [39].

Nb_2O_5 supported on a commercial SiO_2 was also evaluated in this reaction, obtaining the best results for the catalyst with a 20 wt.% of Nb_2O_5, which also displayed the highest acidity [91]. In addition, it was noteworthy that the most active catalyst in the first hours was more susceptible

to suffer deactivation due to the faster formation of carbonaceous deposits. Several research works have reported the coexistence of Lewis and Brönsted sites in the Nb_2O_5 [92]. As has been previously mentioned, the Lewis acid sites interact with primary alcohols, favoring the formation of hydroxyacetone, while the interaction of secondary alcohols with Brönsted acid sites leads to acrolein (Figures 5 and 6) [39]. In addition, these authors established that Brönsted acid sites are also involved in intramolecular reactions, resulting in the formation of coke and consequently provoking the catalytic deactivation [92].

WO_3/ZrO_2 catalysts doped with silica were studied in glycerol dehydration. This tungstated zirconia contained both Brönsted and Lewis acid sites, so the main products are acrolein and hydroxyacetone [64]. It has been suggested that $H^{\delta+}(WO_3)_n{}^{\delta-}$ Brönsted acid sites were responsible for the selectivity toward acrolein [64,93]. Lauriol-Garbey et al. also reported that catalysts doped with silica showed to be more selective and stable catalysts, attaining full conversion and an acrolein yield of 65% after 8 h of TOS (Table 4) [64]. They affirmed that the deposition of SiO_2 on ZrO_2 favored the formation of larger mesopores and reduced the support basicity, minimizing the production of coke precursors, which was crucial to delay the deactivation of catalysts.

5. Conclusions

Different mesoporous materials have been evaluated as solid acid catalysts for glycerol dehydration to acrolein in order to overcome drawbacks associated with deactivation by coke formation. Porous silica-based catalysts, such as mesoporous silica, zeolites, silicon-aluminophosphates, and commercial silica have demonstrated that the presence of mesopores improved catalytic performance. In general, the existence of large pores increases the resistance to pore blocking, since the products diffusion is favored, decreasing the deactivation rate and providing a longer lifetime in the dehydration of glycerol. However, the deactivation of these materials finally took place by coke deposition, since the stability of these mesoporous silicon-based catalysts during their regeneration by thermal treatment was important. Therefore, both the pore size and density of acid sites played an important role in the catalytic performance and deactivation rates, as they were crucial to the control of these parameters to maximize acrolein production.

Author Contributions: Conceptualization, P.M.-T. devised the elaboration of this review. Data curation, J.A.C., C.P.J.-G. and R.M.-T. collected the data reported in the literature previously. Funding adquisition, P.M.-T. obtained the funds coming from the project CTQ2015-64226-C3-3-R. Investigation, J.A.C., C.G.-S. and C.P.J.-G. selected the data of previous research. Project administration, R.M.-T. and C.G.-S. coordinated the research. Supervision, P.M.-T. and R.M.-T. planned the core of the present research. Writing—original draft, J.A.C. wrote the first draft of the present manuscript. Writing—review & editing, C.G.-S., R.M.-T. and P.M.-T. revised and completed the first draft.

Funding: This research was funded by the Ministry of Economy and Competitiveness (Spain), grant numbers (CTQ2015-64226-C3-3-R, IEDI-2016-00743), Junta de Andalucía (Spain) (P12-RNM-1565), and FEDER (European Union) funds.

Acknowledgments: J.A.C. and C.G.-S. thank to the Malaga University for the financial support.

Conflicts of Interest: The authors declare no conflicts of interest.

References

1. Klass, D.L. *Biomass for Renewable Energy, Fuels and Chemicals*; Academic Press: Cambridge, MA, USA, 1998.
2. European Parliament and of the Council. *Directive 2003/30/EC of the European Parliament and of the Council of 05/08/2003 on the Promotion of the Use of Biofuels or Other Renewable Fuels for Transport*; European Parliament and of the Council: Luxembourg, 2003.
3. Ong, H.; Mahlia, T.; Masjuki, H.; Norhasyima, R. Comparison of palm oil, jatropha curcas and calophyllum inophyllum for biodiesel: A review. *Renew. Sustain. Energy Rev.* **2011**, *15*, 3501–3515. [CrossRef]
4. Talebian-Kiakalaieh, A.; Amin, N.; Zarei, A.; Noshadi, I. Transesterification of waste cooking oil by heteropoly acid (HPA) catalyst: Optimization and kinetic model. *Appl. Energy* **2013**, *102*, 283–292. [CrossRef]

5. Tan, H.; Aziz, A.; Aroua, M. Glycerol production and its applications as a raw material: A review. *Renew. Sustain. Energy Rev.* **2013**, *27*, 118–127. [CrossRef]
6. Ciriminna, R.; Della Pina, C.; Rossi, M.; Pagliaro, M. Understanding the glycerol market. *Eur. J. Lipid Sci. Technol.* **2014**, *116*, 1432–1439. [CrossRef]
7. Organisation for Economic Co-Operation and Development/Food and Agriculture Organization of the United Nations (OECD-FAO) Agricultural Outlook 2017–2026. Available online: http://dx.Doi.Org/10.1787/agr_outlook-2017-en (accessed on 21 February 2018).
8. Katryniok, B.; Paul, S.; Belliere-Baca, V.; Rey, P.; Dumeignil, F. Glycerol dehydration to acrolein in the context of new uses of glycerol. *Green Chem.* **2010**, *12*, 2079–2098. [CrossRef]
9. Tsukuda, E.; Sato, S.; Takahashi, R.; Sodesawa, T. Production of acrolein from glycerol over silica-supported heteropoly acids. *Catal. Commun.* **2007**, *8*, 1349–1353. [CrossRef]
10. Pathak, K.; Reddy, K.; Bakhshi, N.; Dalai, A. Catalytic conversion of glycerol to value added liquid products. *Appl. Catal. A Gen.* **2010**, *372*, 224–238. [CrossRef]
11. Werpy, T.; Petersen, G. *Top Value-Added Chemicals from Biomass*; US Department of Energy (USDOE): Washington, DC, USA, 2004; Volume 1.
12. Zhou, C.; Zhao, H.; Tong, D.; Wu, L.; Yu, W. Recent advances in catalytic conversion of glycerol. *Catal. Rev.* **2013**, *55*, 369–453. [CrossRef]
13. Anitha, M.; Kamarudin, S.; Kofli, N. The potential of glycerol as a value-added commodity. *Chem. Eng. J.* **2016**, *295*, 119–130. [CrossRef]
14. Pagliaro, M.; Ciriminna, R.; Kimura, H.; Rossi, M.; Della Pina, C. From glycerol to value-added products. *Angew. Chem. Int. Ed.* **2007**, *46*, 4434–4440. [CrossRef] [PubMed]
15. Liu, L.; Ye, X.; Bozell, J. A comparative review of petroleum-based and bio-based acrolein production. *ChemSusChem* **2012**, *5*, 1162–1180. [CrossRef] [PubMed]
16. Katryniok, B.; Paul, S.; Capron, M.; Dumeignil, F. Towards the sustainable production of acrolein by glycerol dehydration. *ChemSusChem* **2009**, *2*, 719–730. [CrossRef] [PubMed]
17. Pagliaro, M.; Rossi, M. *The Future of Glycerol: New Uses of a Versatile Raw Material*; RSC Publishing: Cambridge, UK, 2008.
18. Chai, S.; Wang, H.; Liang, Y.; Xu, B. Sustainable production of acrolein: Investigation of solid acid-base catalysts for gas-phase dehydration of glycerol. *Green Chem.* **2007**, *9*, 1130–1136. [CrossRef]
19. Tao, L.; Yan, B.; Liang, Y.; Xu, B. Sustainable production of acrolein: Catalytic performance of hydrated tantalum oxides for gas-phase dehydration of glycerol. *Green Chem.* **2013**, *15*, 696–705. [CrossRef]
20. Tao, L.; Chai, S.; Zuo, Y.; Zheng, W.; Liang, Y.; Xu, B. Sustainable production of acrolein: Acidic binary metal oxide catalysts for gas-phase dehydration of glycerol. *Catal. Today* **2010**, *158*, 310–316. [CrossRef]
21. Gu, Y.; Liu, S.; Li, C.; Cui, Q. Selective conversion of glycerol to acrolein over supported nickel sulfate catalysts. *J. Catal.* **2013**, *301*, 93–102. [CrossRef]
22. Cavani, F.; Guidetti, S.; Marinelli, L.; Piccinini, M.; Ghedini, E.; Signoretto, M. The control of selectivity in gas-phase glycerol dehydration to acrolein catalysed by sulfated zirconia. *Appl. Catal. B Environ.* **2010**, *100*, 197–204. [CrossRef]
23. Wang, F.; Dubois, J.; Ueda, W. Catalytic dehydration of glycerol over vanadium phosphate oxides in the presence of molecular oxygen. *J. Catal.* **2009**, *268*, 260–267. [CrossRef]
24. Stosic, D.; Bennici, S.; Sirotin, S.; Calais, C.; Couturier, J.; Dubois, J.; Travert, A.; Auroux, A. Glycerol dehydration over calcium phosphate catalysts: Effect of acidic-basic features on catalytic performance. *Appl. Catal. A Gen.* **2012**, *447*, 124–134. [CrossRef]
25. Suprun, W.; Lutecki, M.; Haber, T.; Papp, H. Acidic catalysts for the dehydration of glycerol: Activity and deactivation. *J. Mol. Catal. A Chem.* **2009**, *309*, 71–78. [CrossRef]
26. Lauriol-Garbey, P.; Postole, G.; Loridant, S.; Auroux, A.; Belliere-Baca, V.; Rey, P.; Millet, J. Acid-base properties of niobium-zirconium mixed oxide catalysts for glycerol dehydration by calorimetric and catalytic investigation. *Appl. Catal. B Environ.* **2011**, *106*, 94–102. [CrossRef]
27. Lauriol-Garbay, P.; Millet, J.; Loridant, S.; Belliere-Baca, V.; Rey, P. New efficient and long-life catalyst for gas-phase glycerol dehydration to acrolein. *J. Catal.* **2011**, *280*, 68–76. [CrossRef]
28. Massa, M.; Andersson, A.; Finocchio, E.; Busca, G.; Lenrick, F.; Wallenberg, L. Performance of ZrO_2-supported Nb- and W-oxide in the gas-phase dehydration of glycerol to acrolein. *J. Catal.* **2013**, *297*, 93–109. [CrossRef]

29. Chai, S.; Yan, B.; Tao, L.; Liang, Y.; Xu, B. Sustainable production of acrolein: Catalytic gas-phase dehydration of glycerol over dispersed tungsten oxides on alumina, zirconia and silica. *Catal. Today* **2014**, *234*, 215–222. [CrossRef]
30. Massa, M.; Andersson, A.; Finocchio, E.; Busca, G. Gas-phase dehydration of glycerol to acrolein over $Al_2O_3^-$, SiO_2^-, and TiO_2-supported Nb- and W-oxide catalysts. *J. Catal.* **2013**, *307*, 170–184. [CrossRef]
31. Ulgen, A.; Hoelderich, W. Conversion of glycerol to acrolein in the presence of WO_3/ZrO_2 catalysts. *Catal. Lett.* **2009**, *131*, 122–128. [CrossRef]
32. Kim, Y.; Jung, K.; Park, E. Gas-phase dehydration of glycerol over ZSM-5 catalysts. *Microporous Mesoporous Mater.* **2010**, *131*, 28–36. [CrossRef]
33. Jia, C.; Liu, Y.; Schmidt, W.; Lu, A.; Schuth, F. Small-sized HZSM-5 zeolite as highly active catalyst for gas phase dehydration of glycerol to acrolein. *J. Catal.* **2010**, *269*, 71–79. [CrossRef]
34. Kim, Y.; Jung, K.; Park, E. A comparative study for gas-phase dehydration of glycerol over H-zeolites. *Appl. Catal. A Gen.* **2011**, *393*, 275–287. [CrossRef]
35. Omata, K.; Izumi, S.; Murayama, T.; Ueda, W. Hydrothermal synthesis of W-Nb complex metal oxides and their application to catalytic dehydration of glycerol to acrolein. *Catal. Today* **2013**, *201*, 7–11. [CrossRef]
36. Oliveira, L.; Portilho, M.; Silva, A.; Taroco, H.; Souza, P. Modified niobia as a bifunctional catalyst for simultaneous dehydration and oxidation of glycerol. *Appl. Catal. B Environ.* **2012**, *117*, 29–35. [CrossRef]
37. Martin, A.; Armbruster, U.; Atia, H. Recent developments in dehydration of glycerol toward acrolein over heteropolyacids. *Eur. J. Lipid Sci. Technol.* **2012**, *114*, 10–23. [CrossRef]
38. Atia, H.; Armbruster, U.; Martin, A. Dehydration of glycerol in gas phase using heteropolyacid catalysts as active compounds. *J. Catal.* **2008**, *258*, 71–82. [CrossRef]
39. Alhanash, A.; Kozhevnikova, E.; Kozhevnikov, I. Gas-phase dehydration of glycerol to acrolein catalysed by caesium heteropoly salt. *Appl. Catal. A Gen.* **2010**, *378*, 11–18. [CrossRef]
40. Kang, T.; Choi, J.; Bang, Y.; Yoo, J.; Song, J.; Joe, W.; Choi, J.; Song, I. Dehydration of glycerin to acrolein over $H_3PW_{12}O_{40}$ heteropolyacid catalyst supported on silica-alumina. *J. Mol. Catal. A Chem.* **2015**, *396*, 282–289. [CrossRef]
41. Laino, T.; Tuma, C.; Curioni, A.; Jochnowitz, E.; Stolz, S. A revisited picture of the mechanism of glycerol dehydration. *J. Phys. Chem. A* **2011**, *115*, 3592–3595. [CrossRef] [PubMed]
42. Kresge, C.; Leonowicz, M.; Roth, W.; Vartuli, J.; Beck, J. Ordered mesoporous molecular-sieves synthesized by a liquid-crystal template mechanism. *Nature* **1992**, *359*, 710–712. [CrossRef]
43. Zhao, D.; Feng, J.; Huo, Q.; Melosh, N.; Fredrickson, G.; Chmelka, B.; Stucky, G. Triblock copolymer syntheses of mesoporous silica with periodic 50 to 300 angstrom pores. *Science* **1998**, *279*, 548–552. [CrossRef] [PubMed]
44. Lourenco, J.; Macedo, M.; Fernandes, A. Sulfonic-functionalized SBA-15 as an active catalyst for the gas-phase dehydration of glycerol. *Catal. Commun.* **2012**, *19*, 105–109. [CrossRef]
45. Dalla Costa, B.O.; Legnoverde, M.; Lago, C.; Decolatti, H.; Querini, C. Sulfonic functionalized SBA-15 catalysts in the gas phase glycerol dehydration. Thermal stability and catalyst deactivation. *Microporous Mesoporous Mater.* **2016**, *230*, 66–75. [CrossRef]
46. Ma, T.; Ding, J.; Shao, R.; Yun, Z. Catalytic conversion of glycerol to acrolein over MCM-41 by the grafting of phosphorus species. *Can. J. Chem. Eng.* **2016**, *94*, 924–930. [CrossRef]
47. Kobayashi, H.; Ito, S.; Hara, K.; Fukuoka, A. Conversion of glycerol to acrolein by mesoporous sulfated zirconia-silica catalyst. *Chin. J. Catal.* **2017**, *38*, 420–425. [CrossRef]
48. Ding, J.; Ma, T.; Yun, Z.; Shao, R. Heteropolyacid ($H_3PW_{12}O_{40}$) supported MCM-41: An effective solid acid catalyst for the dehydration of glycerol to acrolein. *J. Wuhan Univ. Technol.* **2017**, *32*, 1511–1516. [CrossRef]
49. Ma, T.; Ding, J.; Shao, R.; Xu, W.; Yun, Z. Dehydration of glycerol to acrolein over wells-dawson and keggin type phosphotungstic acids supported on MCM-41 catalysts. *Chem. Eng. J.* **2017**, *316*, 797–806. [CrossRef]
50. Liu, R.; Wang, T.; Jin, Y. Catalytic dehydration of glycerol to acrolein over HPW supported on Cs^+ modified SBA-15. *Catal. Today* **2014**, *233*, 127–132. [CrossRef]
51. Liu, R.; Lyu, S.; Wang, T. Sustainable production of acrolein from biodiesel-derived crude glycerol over $H_3PW_{12}O_{40}$ supported on Cs-modified SBA-15. *J. Ind. Eng. Chem.* **2016**, *37*, 354–360. [CrossRef]
52. Ma, T.; Yun, Z.; Xu, W.; Chen, L.; Li, L.; Ding, J.; Shao, R. Pd-$H_3PW_{12}O_{40}$/Zr-MCM-41: An efficient catalyst for the sustainable dehydration of glycerol to acrolein. *Chem. Eng. J.* **2016**, *294*, 343–352. [CrossRef]
53. Trakarnpruk, W. Platinum/phosphotungstic acid/(Zr)MCM-41 catalysts in glycerol dehydration. *Mendeleev Commun.* **2014**, *24*, 167–169. [CrossRef]

54. Viswanadham, B.; Srikanth, A.; Kumar, V.; Chary, K. Vapor phase dehydration of glycerol to acrolein over SBA-15 supported vanadium substituted phosphomolybdic acid catalyst. *J. Nanosci. Nanotechnol.* **2015**, *15*, 5391–5402. [CrossRef] [PubMed]
55. Garcia-Sancho, C.; Moreno-Tost, R.; Merida-Robles, J.; Santamaria-Gonzalez, J.; Jimenez-Lopez, A.; Maireles-Torres, P. Zirconium doped mesoporous silica catalysts for dehydration of glycerol to high added-value products. *Appl. Catal. A Gen.* **2012**, *433*, 179–187. [CrossRef]
56. Katryniok, B.; Paul, S.; Capron, M.; Lancelot, C.; Belliere-Baca, V.; Rey, P.; Dumeignil, F. A long-life catalyst for glycerol dehydration to acrolein. *Green Chem.* **2010**, *12*, 1922–1925. [CrossRef]
57. Cecilia, J.A.; García-Sancho, C.; Mérida-Robles, J.M.; Santamaría-González, J.; Moreno-Tost, R.; Maireles-Torres, P. V and V–P containing Zr-SBA-15 catalysts for dehydration of glycerol to acrolein. *Catal. Today* **2015**, *254*, 43–52. [CrossRef]
58. García-Sancho, C.; Cecilia, J.A.; Moreno-Ruiz, A.; Mérida-Robles, J.M.; Santamaría-González, J.; Moreno-Tost, R.; Maireles-Torres, P. Influence of the niobium supported species on the catalytic dehydration of glycerol to acrolein. *Appl. Catal. B Environ.* **2015**, *179*, 139–149. [CrossRef]
59. Cecilia, J.; Garcia-Sancho, C.; Merida-Robles, J.; Gonzalez, J.; Moreno-Tost, R.; Maireles-Torres, P. WO_3 supported on Zr doped mesoporous SBA-15 silica for glycerol dehydration to acrolein. *Appl. Catal. A Gen.* **2016**, *516*, 30–40. [CrossRef]
60. Garcia-Sancho, C.; Cecilia, J.; Merida-Robles, J.; Gonzalez, J.; Moreno-Tost, R.; Infantes-Molina, A.; Maireles-Torres, P. Effect of the treatment with H_3PO_4 on the catalytic activity of Nb_2O_5 supported on Zr-doped mesoporous silica catalyst. Case study: Glycerol dehydration. *Appl. Catal. B Environ.* **2018**, *221*, 158–168. [CrossRef]
61. Cecilia, J.; Garcia-Sancho, C.; Merida-Robles, J.; Santamaria-Gonzalez, J.; Infantes-Molina, A.; Moreno-Tost, R.; Maireles-Torres, P. Aluminum doped mesoporous silica SBA-15 for glycerol dehydration to value-added chemicals. *J. Sol-Gel Sci. Technol.* **2017**, *83*, 342–354. [CrossRef]
62. Salas, P.; Wang, J.; Armendariz, H.; Angeles-Chavez, C.; Chen, L. Effect of the Si/Zr molar ratio on the synthesis of Zr-based mesoporous molecular sieves. *Mater. Chem. Phys.* **2009**, *114*, 139–144. [CrossRef]
63. Anderson, J.; Fergusson, C.; Rodriguez-Ramos, I.; Guerrero-Ruiz, A. Influence of Si/Zr ratio on the formation of surface acidity in silica-zirconia aerogels. *J. Catal.* **2000**, *192*, 344–354. [CrossRef]
64. Lauriol-Garbey, P.; Loridant, S.; Belliere-Baca, V.; Rey, P.; Millet, J. Gas phase dehydration of glycerol to acrolein over WO_3/ZrO_2 catalysts: Improvement of selectivity and stability by doping with SiO_2. *Catal. Commun.* **2011**, *16*, 170–174. [CrossRef]
65. Katryniok, B.; Paul, S.; Capron, M.; Belliere-Baca, V.; Rey, P.; Dumeignil, F. Regeneration of silica-supported silicotungstic acid as a catalyst for the dehydration of glycerol. *ChemSusChem* **2012**, *5*, 1298–1306. [CrossRef] [PubMed]
66. Carrico, C.; Cruz, F.; Santos, M.; Pastore, H.; Andrade, H.; Mascarenhas, A. Efficiency of zeolite MCM-22 with different SiO_2/Al_2O_3 molar ratios in gas phase glycerol dehydration to acrolein. *Microporous Mesoporous Mater.* **2013**, *181*, 74–82. [CrossRef]
67. Choi, Y.; Park, H.; Yun, Y.; Yi, J. Effects of catalyst pore structure and acid properties on the dehydration of glycerol. *ChemSusChem* **2015**, *8*, 974–979. [CrossRef] [PubMed]
68. Rodrigues, M.; Vignatti, C.; Garetto, T.; Pulcinelli, S.; Santilli, C.; Martins, L. Glycerol dehydration catalyzed by MWW zeolites and the changes in the catalyst deactivation caused by porosity modification. *Appl. Catal. A Gen.* **2015**, *495*, 84–91. [CrossRef]
69. Gu, Y.; Cui, N.; Yu, Q.; Li, C.; Cui, Q. Study on the influence of channel structure properties in the dehydration of glycerol to acrolein over H-zeolite catalysts. *Appl. Catal. A Gen.* **2012**, *429*, 9–16. [CrossRef]
70. Possato, L.; Cassinelli, W.; Garetto, T.; Pulcinelli, S.; Santilli, C.; Martins, L. One-step glycerol oxidehydration to acrylic acid on multifunctional zeolite catalysts. *Appl. Catal. A Gen.* **2015**, *492*, 243–251. [CrossRef]
71. Decolatti, H.P.; Dalla Costa, B.O.; Querini, C.A. Dehydration of glycerol to acrolein using H-ZSM5 zeolite modified by alkali treatment with Naoh. *Microporous Mesoporous Mater.* **2015**, *204*, 180–189. [CrossRef]
72. Possato, L.; Diniz, R.; Garetto, T.; Pulcinelli, S.; Santilli, C.; Martins, L. A comparative study of glycerol dehydration catalyzed by micro/mesoporous MFI zeolites. *J. Catal.* **2013**, *300*, 102–112. [CrossRef]
73. Wang, Z.; Wang, L.; Jiang, Y.; Hunger, M.; Huang, J. Cooperativity of Brönsted and Lewis acid sites on zeolite for glycerol dehydration. *ACS Catal.* **2014**, *4*, 1144–1147. [CrossRef]

74. Lari, G.; Chen, Z.; Mondelli, C.; Perez-Ramirez, J. Bifunctional hierarchical zeolite-supported silver catalysts for the conversion of glycerol to allyl alcohol. *ChemCatChem* **2017**, *9*, 2195–2202. [CrossRef]
75. Zhang, H.; Hu, Z.; Huang, L.; Zhang, H.; Song, K.; Wang, L.; Shi, Z.; Ma, J.; Zhuang, Y.; Shen, W.; et al. Dehydration of glycerol to acrolein over hierarchical zsm-5 zeolites: Effects of mesoporosity and acidity. *ACS Catal.* **2015**, *5*, 2548–2558. [CrossRef]
76. Beerthuis, R.; Huang, L.; Shiju, N.; Rothenberg, G.; Shen, W.; Xu, H. Facile synthesis of a novel hierarchical ZSM-5 zeolite: A stable acid catalyst for dehydrating glycerol to acrolein. *ChemCatChem* **2018**, *10*, 211–221. [CrossRef] [PubMed]
77. Huang, L.; Qin, F.; Huang, Z.; Zhuang, Y.; Ma, J.; Xu, H.; Shen, W. Hierarchical ZSM-5 zeolite synthesized by an ultrasound-assisted method as a long-life catalyst for dehydration of glycerol to acrolein. *Ind. Eng. Chem. Res.* **2016**, *55*, 7318–7327. [CrossRef]
78. Dos Santos, M.; Andrade, H.; Mascarenhas, A. Reduced coke formation during the gas phase oxidative dehydration of glycerol over ferrierite zeolites synthesized in fluoride medium. *Microporous Mesoporous Mater.* **2016**, *223*, 105–113. [CrossRef]
79. Viswanadham, B.; Nagaraju, N.; Rohitha, C.; Vishwanathan, V.; Chary, K. Synthesis, characterization and catalytic dehydration of glycerol to acrolein over phosphotungstic acid supported Y-zeolite catalysts. *Catal. Lett.* **2018**, *148*, 397–406. [CrossRef]
80. Silva, T.; dos Santos, M.; Santiago, A.; Santana, D.; Cruz, F.; Andrade, H.; Mascarenhas, A. Gas phase glycerol oxidative dehydration over bifunctional V/H-zeolite catalysts with different zeolite topologies. *Catal. Today* **2017**, *289*, 38–46. [CrossRef]
81. Pestana, C.; Guerra, A.; Ferreira, G.; Turci, C.; Mota, C. Oxidative dehydration of glycerol to acrylic acid over vanadium-impregnated zeolite beta. *J. Braz. Chem. Soc.* **2013**, *24*, 100–105. [CrossRef]
82. Wilson, S.; Lok, B.; Messina, C.; Cannan, T.; Flanigen, E. Aluminophosphate molecular-sieves. A new class of microporous crystalline inorganic solids. *J. Am. Chem. Soc.* **1982**, *104*, 1146–1147. [CrossRef]
83. Sastre, G.; Lewis, D.; Catlow, C. Mechanisms of silicon incorporation in aluminophosphate molecular sieves. *J. Mol. Catal. A Chem.* **1997**, *119*, 349–356. [CrossRef]
84. Lourenco, J.; Fernandes, A.; Bertolo, R.; Ribeiro, M. Gas-phase dehydration of glycerol over thermallystable sapo-40 catalyst. *RSC Adv.* **2015**, *5*, 10667–10674. [CrossRef]
85. Fernandes, A.; Filipa Ribeiro, M.; Lourenço, J.P. Gas-phase dehydration of glycerol over hierarchical silicoaluminophosphate sapo-40. *Catal. Commun.* **2017**, *95*, 16–20. [CrossRef]
86. Kozhevnikov, I. Catalysis by heteropolyacids and multicomponent polyoxometalates in liquid-phase reactions. *Chem. Rev.* **1998**, *98*, 171–198. [CrossRef] [PubMed]
87. Thomas, A.; Dablemont, C.; Basset, J.; Lefebvre, F. Comparison of $H_3PW_{12}O_{40}$ and $H_4SiW_{12}O_{40}$ heteropolyacids supported on silica by h-1 mas nmr. *C. R. Chim.* **2005**, *8*, 1969–1974. [CrossRef]
88. Kim, Y.; You, S.; Jung, K.; Park, E. Effect of al content on the gas-phase dehydration of glycerol over silica-alumina-supported silicotungstic acid catalysts. *Bull. Korean Chem. Soc.* **2012**, *33*, 2369–2377. [CrossRef]
89. Kim, Y.; Jung, K.; Park, E. Gas-phase dehydration of glycerol over silica-alumina catalysts. *Appl. Catal. B Environ.* **2011**, *107*, 177–187. [CrossRef]
90. Chai, S.; Wang, H.; Liang, Y.; Xu, B. Sustainable production of acrolein: Gas-phase dehydration of glycerol over 12-tungstophosphoric acid supported on ZrO_2 and SiO_2. *Green Chem.* **2008**, *10*, 1087–1093. [CrossRef]
91. Shiju, N.; Brown, D.; Wilson, K.; Rothenberg, G. Glycerol valorization: Dehydration to acrolein over silica-supported niobia catalysts. *Top. Catal.* **2010**, *53*, 1217–1223. [CrossRef]
92. Foo, G.; Wei, D.; Sholl, D.; Sievers, C. Role of Lewis and Brönsted acid sites in the dehydration of glycerol over niobia. *ACS Catal.* **2014**, *4*, 3180–3192. [CrossRef]
93. Baertsch, C.; Komala, K.; Chua, Y.; Iglesia, E. Genesis of Brönsted acid sites during dehydration of 2-butanol on tungsten oxide catalysts. *J. Catal.* **2002**, *205*, 44–57. [CrossRef]